Spin expansion for binary black hole mergers: New predictions and future directions

Latham Boyle and Michael Kesden

Canadian Institute for Theoretical Astrophysics (CITA), Canada

(Received 13 February 2008; published 10 July 2008)

In a recent paper [L. Boyle, M. Kesden, and S. Nissanke, Phys. Rev. Lett. **100**, 151101 (2008)], we introduced a spin expansion that provides a simple yet powerful way to understand aspects of binary black hole merger. This approach relies on the symmetry properties of initial and final quantities like the black hole mass m, kick velocity $\mathbf{k}$, and spin vector $\mathbf{s}$, rather than a detailed understanding of the merger dynamics. In this paper, we expand on this proposal, examine how well its predictions agree with current simulations, and discuss several future directions that would make it an even more valuable tool. The spin expansion yields many new predictions, including several *exact* results that may be useful for testing numerical codes. Some of these predictions have already been confirmed, while others await future simulations. We explain how a relatively small number of simulations—10 equal-mass simulations, and 16 unequal-mass simulations—may be used to calibrate all of the coefficients in the spin expansion up to second order at the minimum computational cost. For a more general set of simulations of given covariance, we derive the minimum-variance unbiased estimators for the spin-expansion coefficients. We discuss how this calibration would be interesting and fruitful for general relativity and astrophysics. Finally, we sketch the extension to eccentric orbits.

DOI: 10.1103/PhysRevD.78.024017 PACS numbers: 04.70.Bw, 04.25.dg, 97.60.Lf

I. INTRODUCTION

Binary black hole (BBH) merger—in which two spinning black holes inspiral due to the emission of gravitational radiation and eventually merge to form a single spinning black hole—is one of the most important problems in classical general relativity, and has significant ramifications for astrophysics, cosmology, and gravitational-wave observations. For decades, analytical and numerical approaches to the BBH merger problem have been frustrated by conceptual and technical difficulties associated with solving the nonlinear Einstein equations—especially during the last few orbits and final plunge, when the "luminosity" in gravitational radiation is highest. Dramatic progress came in 2005, as new insights and increased computational resources finally allowed numerical relativists to simulate the *entire* merger—including the last few orbits of inspiral, the plunge, the formation of a common event horizon, and the ringdown of the final Kerr black hole [1–3]. Following this breakthrough, simulations of BBH merger have produced a number of remarkable results.

The most surprising and interesting results have been obtained just within the past year, from simulations of merging black holes with large initial spins [4–23]. The result that has received the most attention is that highly-spinning initial black holes can merge to form a final black hole with an enormous recoil velocity—as large as 4000 km/s—relative to the binary's center-of-momentum frame [4–6]. The idea of a supermassive black hole rocketing through its host galaxy at such a speed has understandably caught the attention of many astrophysicists.

In this paper, we highlight a second surprising result. Despite the complicated and nonlinear dynamics of the merger process, the final state of the merger seems, in some sense, to be an unexpectedly simple and smooth function of the initial state of the binary. We would like to make this statement more quantitative and precise.

In a recent paper [24], we introduced a "spin-expansion" formalism for understanding aspects of BBH merger. We expand on this proposal in several ways in the present paper. Here is a recap of the basic idea. Even though the merger is a messy nonlinear process, it is useful to regard it as a map from a simple initial state (two well separated Kerr black holes with mass ratio $q \equiv M_b/M_a$ and dimensionless spins $\mathbf{a}$ and $\mathbf{b}$) to a simple final state (a final Kerr black with mass m, spin vector $\mathbf{s}$ and kick velocity $\mathbf{k}$). Given any final quantity f (e.g. m, $\mathbf{k}$, or $\mathbf{s}$), we can Taylor expand the function $f(q, \mathbf{a}, \mathbf{b})$ around $\mathbf{a} = \mathbf{b} = 0$, and use symmetry arguments to dramatically reduce the number of independent terms at each order. When compared with published simulation results, this "spin expansion" seems to rapidly converge: the leading-order terms yield a surprisingly good first approximation, the next-to-leading-order terms give an even better approximation, and so on. In the present paper, we present these points in detail, and explore some of their implications and extensions.

A. Some advantages of the spin expansion

How does the spin expansion complement other approaches to the BBH merger problem?

1. First, it is *simple*. Previous approaches—notably the post-Newtonian approximation and full numerical relativity—are highly technical and sophisticated and have taken decades to develop. By contrast, we believe that the deri-

 © 2008 The American Physical Society

vations in this paper will be accessible, even to physicists with no prior expertise in this area.

2. Second, it is *general*. In this paper, we focus on applying the spin expansion to the final black hole's mass, kick, and spin (m, $\mathbf{k}$, $\mathbf{s}$), but we expect that analogous arguments may be useful for studying *any* other final observable with well defined transformation properties under the simple symmetries $\{R, P, X\}$ discussed below. This may also include the multipoles of the gravitational-wave signal emitted by the binary—this is currently a speculation, and remains a topic for future work.

3. Third, it is *conceptually distinct*. Previous approaches attempt to follow the *dynamics* of the merger—by solving the Einstein equations numerically, or through some analytical approximation. By contrast, our approach is to consider the map directly from the initial state to the final state, and thereby "leap over" the complicated merger dynamics in between. To constrain this map, we rely purely on *symmetry* arguments, together with the *assumption* (supported by simulations) that the Taylor expansion of the map around $\mathbf{a} = \mathbf{b} = 0$ converges rapidly. Therefore, our approach clarifies which aspects of the final state are due to the complicated nonlinearities of Einstein's equations, and which aspects follow from more elementary considerations.

4. Fourth, it is *practical* for cosmological and astrophysical applications. For example, a cosmological simulation of galaxy merger may also wish to track the corresponding supermassive black holes, since their feedback may be important for galactic structure and evolution. Of course, it would be hopeless to follow the BBH dynamics in detail—the dynamical time near final merger is too short relative to the other time scales in the problem. Instead, one is likely to resort to a simplifying algorithm: e.g. when the two holes get sufficiently close, they are replaced by a single hole with appropriate quantities $\{m, \mathbf{k}, \mathbf{s}\}$. The fact that the spin expansion maps the initial state (well before merger) directly to the final state (well after merger) makes it well suited for these types of problems.

5. Fifth, it is *efficient*. To fully specify the initial BBH spin configuration, we must specify 6 numbers—3 components each for the initial spins $\mathbf{a}$ and $\mathbf{b}$. What is the most economical way to map out this 6-dimensional space with numerical simulations? If we crudely put 10 grid points along each direction, we would need 10^6 simulations—an impossibly large value, since each simulation is very computationally expensive. On the other hand, we can use the spin expansion to map out the *same* 6-dimensional space, at second- or third-order accuracy, with only $\mathcal{O}(10)$ simulations—a huge computational savings. This issue is treated in detail in Sec. V. In this sense, the spin expansion acts like a kind of "data compression," describing the 6-dimensional space of initial spins more succinctly, without *oversimplifying* it.

6. Sixth, it is *valid through the entire merger*. The spin expansion is based on *exact* symmetries of general relativity, which are equally valid during all stages of BBH merger: inspiral, plunge, and ringdown. Hence, it is particularly well suited for questions about how the final state depends on the initial state in BBH merger. By contrast, the post-Newtonian approximation is an expansion of the Einstein equations in v/c, and treats BBHs as pairs of interacting point particles. It breaks down during the late stages of the merger—the last orbits, plunge, and ringdown, when the black holes begin to orbit with relativistic velocities and then cease to be two separate entities. Since these late stages emit gravitational waves copiously, and play a crucial role in determining the properties of the final black hole, the post-Newtonian formalism is *not* well suited for predicting the final state of BBH merger. (On the other hand, it is excellently suited for describing the binary and its gravitational-wave emission when the black holes are well separated and orbiting nonrelativistically.)

7. Seventh, it is *predictive*. As we show in detail in this paper, the spin expansion makes a host of detailed (and successful) quantitative predictions for the results of simulations. Many of these predictions are new and distinct from the predictions of other analytical approaches. They reveal interesting features of the simulations that might not have been noticed otherwise.

8. These predictions are *derived*—they are not guesses. This is to be contrasted with expressions for the final kick velocity [5,7–9] which were *inspired* by post-Newtonian equations, but are ultimately empirical fitting formulas which are *not* derived. Indeed, if these formulas continued to hold in general, it would be quite amazing. They are linear in the initial spins, and we will highlight several effects which appear to be quintessentially nonlinear in the spins, and hence *not* captured by the post-Newtonian-inspired fitting formulas.

In this subsection, we have made an aggressive case for the merits of the spin expansion. We must also stress the obvious point that the spin expansion merely *complements* the other approaches to BBH merger—it does not replace them. It should be clear that numerical simulations, post-Newtonian techniques, and post-Newtonian-inspired fitting formulas offer a huge amount of dynamical information and insights which cannot be obtained from the spin expansion alone. Nonetheless, the spin expansion provides unique understanding, as we hope will become clear in the course of this paper.

B. Observational motivations

The process of BBH merger is of great observational interest, since it is expected to govern the final evolution of both *stellar-mass* BBHs (produced in stellar collapse) and *supermassive* BBHs (produced whenever galaxies merge).

Gravitational waves from merging stellar-mass BBHs are an important source for the ground-based detector LIGO [25], while gravitational waves from merging supermassive BBHs are a primary source for the space-based detector LISA [26]. These gravitational waves will provide unprecedented tests of strong-field general relativity, and open a new window onto exotic and previously invisible astrophysical phenomena. For example, after the two initial black holes form a common event horizon, they are predicted to "ring down" (like a bell) to a final quiescent Kerr black hole. This ringdown signal is an important observable for future gravitational-wave detectors, and may be thought of as a superposition of so-called "quasinormal modes." The observed spectrum of quasinormal modes depends on the quantities $\{m, \mathbf{k}, \mathbf{s}\}$ characterizing the final black hole, so the ability to predict these quantities may play an important role in interpreting these observations.

The quantities $\{m, \mathbf{k}, \mathbf{s}\}$ characterizing the final black hole are also interesting astrophysically. These quantities may be probed observationally via the x-ray spectrum emitted from the inner edge of the accretion disk around a black hole. From the standpoint of *supermassive* BBH merger, they are believed to be linked to a variety of observables, including: (i) the quasar luminosity function [27,28]; (ii) the location of a quasar with respect to its host galaxy [29]; (iii) the orientation and shape of jets in active galactic nuclei [30,31]; (iv) the correlation between black hole mass and velocity dispersion in the surrounding stellar bulge [32,33]; (v) the density profile in the centers of galaxies [34,35]. Supermassive BBH merger is part of an interconnected web of astrophysical issues—the structure of this web is still poorly understood, and many fascinating questions remain.

Finally, since the present paper is concerned with the merger of *spinning* black holes, we should note that many—perhaps even *most*—astrophysical black holes are indeed expected to have significant spin. On theoretical grounds, black holes grown by gas accretion are expected to have spins near the maximum Kerr limit [36,37]. These predictions are supported by recent observations of active galactic nuclei by the x-ray observatory *XMM-Newton*. Features in the Fe-Kα line of the Seyfert 1.2 galaxy MCG–06-30-15 are best modeled by a black hole with Kerr parameter $a = 0.989^{+0.009}_{-0.002}$ at 90% confidence (where $a = 1$ would correspond to the maximal Kerr value) [38]. Other observations suggesting significant black hole spin include [39,40]. While torques from accreting gas tend to align the orbital and spin angular momenta with the large-scale gas flow in gas-rich "wet" mergers [41], no such mechanisms exist in gas-poor "dry" mergers [42] making studies of generic initial BBH spin configurations essential for understanding these systems.

C. Outline of this paper

This paper is organized as follows. In Sec. II we review the formalism of the spin expansion introduced in our Letter [24]. We use this formalism in Sec. III to identify several particularly symmetric initial spin configurations for which a subset of the final quantities $f \in \{m, s_i, k_i\}$ *identically* vanish. These configurations may be useful to numerical relativists to help identify systematic errors in their codes that violate these symmetry constraints. We compare the predictions of our spin expansion to simulations of these configurations and some less symmetric ones in Sec. IV. Not only is the spin expansion *consistent* with all existing simulations, but it allows us to discover *qualitatively new* nonlinear effects by specifying the spin dependence these effects must take. These *nonlinear* spin effects reveal the inadequacy of existing "Kidder" fitting formulas for kick velocities [5,43] modeled after the purely *linear* terms in post-Newtonian expressions for the instantaneous loss of linear momentum. Though existing simulations verify these exciting predictions of the spin expansion, they fail to fully constrain many of the terms at second order and beyond. In Sec. V, we propose a new series of simulations that will allow us to calibrate the coefficients of all terms to second order. We hope that the promise of our approach and its successes described in this paper will motivate numerical relativists to undertake these simulations in the near future. Finally, in Sec. VI, we take stock of what has been accomplished in this paper and what remains to be done.

Supplementary information has been organized into a series of appendices. We compile the relevant results of recently published simulations for convenience in Appendix A. Lengthy equations relating different spin expansions in Sec. IV are relegated to Appendix B for clarity of presentation. Appendix C provides third-order terms in the spin expansion to extend the second-order calibration procedure described in Sec. V. In Appendix D we show how systematic uncertainties in simulations affect our estimates of the coefficients in the spin expansion. In particular, for a general set of simulations of given covariance, we derive the minimum-variance unbiased estimators for the spin-expansion coefficients. Finally, in Appendix E, we briefly remark on the generalization of the spin expansion to initially eccentric orbits.

II. THE SPIN-EXPANSION FORMALISM

For a brisk introduction to the spin expansion, see the first two pages of [24]. In this section, we introduce the same formalism at a more leisurely pace, providing more detailed explanations along the way.[1]

[1]If you find the presentation in this section suspiciously simplistic or Newtonian, we request your patience. Although we regard this simplicity as one of the key virtues of the spin expansion, in a forthcoming paper we make contact with the full 3 + 1 formulation of general relativity, and also with the post-Newtonian expansion. In the meantime, the proof is in the pudding: we hope that Sec. IV will convince you that the spin expansion is powerfully explanatory and predictive when compared with existing simulations.

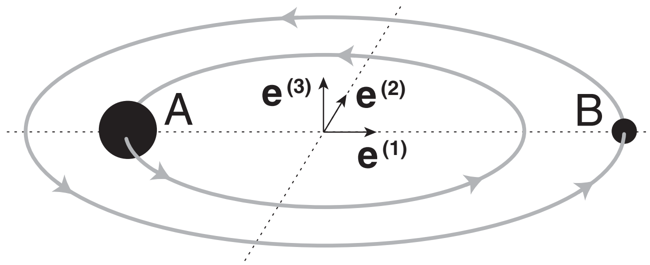

FIG. 1. A BBH system, including the orthonormal triad defined in the text.

A. Preliminaries

Imagine two black holes A and B in a circular orbit,[2] as shown in Fig. 1. Assume that A and B are initially far apart—far enough that they may be thought of as two Kerr black holes, characterized by masses (M_a, M_b) and spins $(\mathbf{S}_a, \mathbf{S}_b)$. Let us work in the center-of-momentum frame of the complete system (including the gravitational radiation, and the momentum that it carries). The orbit gradually shrinks due to gravitational-wave emission, until A and B eventually merge. After the merger, the spacetime quickly settles down to a final Kerr black hole with mass M_f, spin $\mathbf{S}_f$, and recoil velocity (or "kick velocity") $\mathbf{k}$ relative to the center-of-momentum frame.

Next recall that classical general relativity has a trivial one-parameter rescaling symmetry. Starting from a given solution, we can obtain another solution by rescaling every physical quantity X according to its mass dimension d_X: $X \to \lambda^{d_X} X$, where λ is an arbitrary positive number.[3] Of course, rescaling the solution in this way is closely related to rescaling the basic unit of mass. For our purposes, this freedom is more distracting than interesting: from now on, we will work exclusively with *dimensionless* quantities, which are unaffected by such a rescaling. In particular, it is useful to define the dimensionless initial mass ratio

$$q \equiv M_b/M_a, \tag{1}$$

the dimensionless initial spins

$$\mathbf{a} \equiv \mathbf{S}_a/M_a^2, \qquad \mathbf{b} \equiv \mathbf{S}_b/M_b^2, \tag{2}$$

the dimensionless final mass

$$m \equiv M_f/(M_a + M_b), \tag{3}$$

and the dimensionless final spin

$$\mathbf{s} \equiv \mathbf{S}_f/M_f^2. \tag{4}$$

B. Initial configuration of a black hole binary

To fully specify the initial configuration of this binary system, how much information do we need to provide?

Since we are only interested in dimensionless quantities, we can fully specify the initial state of the binary in terms of 8 numbers $\{\psi, q, a_i, b_i\}$ as follows. First choose an inspiral parameter ψ, by which we mean a dimensionless quantity that varies monotonically along the orbit of the binary during the adiabatic inspiral phase. For example, ψ could be the (dimensionless) orbital separation $r/(M_a + M_b)$, or the (dimensionless) magnitude of the orbital angular momentum $L/(M_a + M_b)^2$. At the "initial instant" (i.e. at some particular value of ψ), define an orthonormal triad $\{\mathbf{e}^{(1)}, \mathbf{e}^{(2)}, \mathbf{e}^{(3)}\}$ as shown in Fig. 1: $\mathbf{e}^{(3)}$ points along the orbital angular momentum, $\mathbf{e}^{(1)}$ points from A to B, and $\mathbf{e}^{(2)} = \mathbf{e}^{(3)} \times \mathbf{e}^{(1)}$. This same triad is conventionally introduced in post-Newtonian studies of spinning compact binaries (see e.g. [49–52]). Now we can specify the initial state of the binary, at the initial instant ψ, by giving 7 more numbers—namely, the dimensionless mass ratio q, and the initial spin components

$$a_i \equiv \mathbf{a} \cdot \mathbf{e}^{(i)}, \qquad b_i \equiv \mathbf{b} \cdot \mathbf{e}^{(i)} \tag{5}$$

relative to the orthonormal triad.

We can think of the 7 numbers $\{q, a_i, b_i\}$ as parametrizing the 7-dimensional space of physically-distinct black hole binaries (in circular orbit). Each "point" in this 7-dimensional space corresponds to an inspiral trajectory. On each trajectory, there is an initial instant labeled by ψ, at which the 7 numbers $\{q, a_i, b_i\}$ are to be specified.

C. Symmetry considerations for binary systems

Now let us consider how various final (postmerger) quantities can depend on the initial quantities presented in the previous subsection.

Long after the merger, let f denote a final quantity of interest. For the purposes of illustration, we will focus in this section on a particular set of final quantities $f \in \{m, k_i, s_i\}$—namely, the final Kerr black hole's dimensionless mass m, and the components

$$k_i \equiv \mathbf{k} \cdot \mathbf{e}^{(i)}, \qquad s_i \equiv \mathbf{s} \cdot \mathbf{e}^{(i)} \tag{6}$$

of its final kick and spin—relative to the orthonormal triad defined at the initial time ψ as explained in the previous subsection. Our presentation will hopefully be general enough to make it clear how to apply the same formalism to various other final quantities of interest, such as the

[2] Gravitational radiation carries away energy more efficiently than angular momentum, and hence circularizes BBH orbits [44]. Thus, most astrophysically relevant systems are expected to circularize long before merger. With the exception of a few papers (e.g. [43,45–48]), simulations of BBH mergers thus far have focused on circular orbits. Nevertheless, in Appendix E, we will explain the extension of our formalism to noncircular (eccentric) orbits.

[3] Throughout this paper, we work in "geometrical units" with $G_N = c = 1$, so that each physical quantity has units of mass to some power, called its "mass dimension." For example, angular momentum has mass dimension $= 2$, while distance and time both have mass dimension $= 1$.

(dimensionless) total radiated energy $\epsilon_{\rm rad} \equiv E_{\rm rad}/(M_a + M_b)$, or the (dimensionless) total radiated angular momentum $\mathbf{j}_{\rm rad} \equiv \mathbf{J}_{\rm rad}/(M_a + M_b)^2$.

Any dimensionless final quantity f is a function of the initial quantities $\{q, a_i, b_i\}$ and the initial instant ψ at which these quantities were specified,

$$f = f(\psi, q, a_i, b_i). \tag{7}$$

The goal of this section is to constrain the function $f(\psi, q, a_i, b_i)$ as much as possible, using symmetry arguments alone. We will consider 3 simple transformations of the binary system: rotation " R," parity " P," and exchange " X." Once we know how the initial and final quantities transform under R, P, and X, we can constrain the map $f(\psi, q, a_i, b_i)$ by requiring it to relate initial quantities to final ones in a way consistent with their respective transformation laws.

First consider the transformations R and P. R is a global 3-dimensional rotation of the entire binary system (as if it were a single rigid body), and P is a global parity transformation which reflects every point in the binary through the origin (the center of mass). How do the initial quantities $\{\psi, q, a_i, b_i\}$ transform under R and P? The quantities $\{\mathbf{e}^{(1)}, \mathbf{e}^{(2)}\}$ are both *vectors*, while the quantities $\{\mathbf{e}^{(3)}, \mathbf{a}, \mathbf{b}\}$ are all *pseudovectors*. The dot product of two vectors or two pseudovectors is a *scalar*, which is invariant under both R and P. The dot product of a vector and a pseudovector is a *pseudoscalar*, which is invariant under R and flips sign under P. Thus, the quantities $\{a_1, a_2, b_1, b_2\}$ are pseudoscalars, while the quantities $\{a_3, b_3\}$ are scalars. In summary, the initial spin components transform under P as

$$a_i \rightarrow \tilde{a}_i, \qquad b_i \rightarrow \tilde{b}_i, \tag{8}$$

where we have introduced the convenient notation

$$\tilde{a}_i \equiv \{-a_1, -a_2, +a_3\}, \qquad \tilde{b}_i \equiv \{-b_1, -b_2, +b_3\}. \tag{9}$$

Note that the initial mass ratio q is also a scalar, and the parameter ψ may be chosen to be a scalar: for example, the magnitude $r/(M_a + M_b)$ of the initial separation, or the magnitude $L/(M_a + M_b)^2$ of the initial orbital angular momentum.

For the rest of this paper, we restrict our attention to final quantities f that are either scalars (like $\{m, k_1, k_2, s_3\}$) or pseudoscalars (like $\{s_1, s_2, k_3\}$). In other words, we focus on final quantities f that are invariant under R, and transform under P as

$$f \rightarrow (\pm)_P f, \tag{10}$$

where $(\pm)_P = +1$ when f is a scalar, and $(\pm)_P = -1$ when f is a pseudoscalar. The function $f(\psi, q, a_i, b_i)$ automatically respects R (since the initial and final quantities are both invariant under R). In order to be consistent with P, it must satisfy the constraint

$$f(\psi, q, a_i, b_i) = (\pm)_P f(\psi, q, \tilde{a}_i, \tilde{b}_i). \tag{11}$$

Finally consider an "exchange transformation" X, which leaves the physical system absolutely unchanged, but simply swaps the labels of the two black holes, $A \leftrightarrow B$. How do the initial quantities $\{\psi, q, a_i, b_i\}$ transform under X? The parameter ψ is invariant, and the mass ratio transforms as $q \rightarrow 1/q$. The initial spin vectors are swapped, $\mathbf{a} \leftrightarrow \mathbf{b}$, while the triad elements transform as

$$\{\mathbf{e}^{(1)}, \mathbf{e}^{(2)}, \mathbf{e}^{(3)}\} \rightarrow \{-\mathbf{e}^{(1)}, -\mathbf{e}^{(2)}, +\mathbf{e}^{(3)}\}. \tag{12}$$

Therefore the initial spin components transform as

$$a_i \rightarrow \tilde{b}_i, \qquad b_i \rightarrow \tilde{a}_i. \tag{13}$$

Now suppose that the final quantity f transforms under X as

$$f \rightarrow (\pm)_X f, \tag{14}$$

where $(\pm)_X = +1$ when f is "even" under exchange (like $\{k_3, s_3, m\}$), and $(\pm)_X = -1$ when f is "odd" under exchange (like $\{k_1, k_2, s_1, s_2\}$). In order to be consistent with X, the function $f(\psi, q, a_i, b_i)$ must satisfy the constraint

$$f(\psi, q, a_i, b_i) = (\pm)_X f(\psi, 1/q, \tilde{b}_i, \tilde{a}_i). \tag{15}$$

Equivalently, but more conveniently, if f transforms under the combined transformation PX as

$$f \rightarrow (\pm)_{PX} f, \tag{16}$$

then the function $f(\psi, q, a_i, b_i)$ must satisfy the constraint

$$f(\psi, q, a_i, b_i) = (\pm)_{PX} f(\psi, 1/q, b_i, a_i). \tag{17}$$

Note that $(\pm)_{PX}$ is just given by the product

$$(\pm)_{PX} = (\pm)_P (\pm)_X. \tag{18}$$

We emphasize that Eqs. (11) and (17) capture the key results of this subsection. To illustrate these formulas, let us apply them to the final quantities $f \in \{m, k_i, s_i\}$.

First, in Table I, we collect the corresponding values of $(\pm)_P$, $(\pm)_X$, and $(\pm)_{PX}$ for $f \in \{m, k_i, s_i\}$. These values are easy to check. For example, consider the component $s_1 = \mathbf{s} \cdot \mathbf{e}^{(1)}$. Under a parity transformation P, the pseudovector quantity $\mathbf{s}$ (an angular momentum) is unchanged, while the vector quantity $\mathbf{e}^{(1)}$ (the direction from A to B) flips sign, so their dot product s_1 is a pseudoscalar: $(\pm)_P = -1$. Under an exchange transformation X, which merely changes the labels $A \leftrightarrow B$, the final angular momentum $\mathbf{s}$ is clearly unchanged, but the triad element $\mathbf{e}^{(1)}$ (the direction from

TABLE I. Transformation under P, X, and PX, for various final quantities f.

f	m, s_3	s_1, s_2	k_1, k_2	k_3
$(\pm)_P$	+	−	+	−
$(\pm)_X$	+	−	−	+
$(\pm)_{PX}$	+	+	−	−

A to B) flips sign, so their dot product s_1 is odd under exchange: $(\pm)_X = -1$.

Now, using Eq. (11), together with the $(\pm)_P$ row in Table I, we find that parity P implies that the final quantities $f \in \{m, k_i, s_i\}$ must obey the following constraints:

$$m(\psi, q, a_i, b_i) = +m(\psi, q, \tilde{a}_i, \tilde{b}_i), \tag{19a}$$

$$\begin{aligned} k_1(\psi, q, a_i, b_i) &= +k_1(\psi, q, \tilde{a}_i, \tilde{b}_i),\\ k_2(\psi, q, a_i, b_i) &= +k_2(\psi, q, \tilde{a}_i, \tilde{b}_i),\\ k_3(\psi, q, a_i, b_i) &= -k_3(\psi, q, \tilde{a}_i, \tilde{b}_i), \end{aligned} \tag{19b}$$

$$\begin{aligned} s_1(\psi, q, a_i, b_i) &= -s_1(\psi, q, \tilde{a}_i, \tilde{b}_i),\\ s_2(\psi, q, a_i, b_i) &= -s_2(\psi, q, \tilde{a}_i, \tilde{b}_i),\\ s_3(\psi, q, a_i, b_i) &= +s_3(\psi, q, \tilde{a}_i, \tilde{b}_i). \end{aligned} \tag{19c}$$

Using Eq. (17), together with the $(\pm)_{PX}$ row in Table I, we find that exchange symmetry (or, more correctly, PX) implies that the final quantities $f \in \{m, k_i, s_i\}$ must obey the following constraints:

$$m(\psi, q, a_i, b_i) = +m(\psi, 1/q, b_i, a_i), \tag{20a}$$

$$\begin{aligned} k_1(\psi, q, a_i, b_i) &= -k_1(\psi, 1/q, b_i, a_i),\\ k_2(\psi, q, a_i, b_i) &= -k_2(\psi, 1/q, b_i, a_i),\\ k_3(\psi, q, a_i, b_i) &= -k_3(\psi, 1/q, b_i, a_i), \end{aligned} \tag{20b}$$

$$\begin{aligned} s_1(\psi, q, a_i, b_i) &= +s_1(\psi, 1/q, b_i, a_i),\\ s_2(\psi, q, a_i, b_i) &= +s_2(\psi, 1/q, b_i, a_i),\\ s_3(\psi, q, a_i, b_i) &= +s_3(\psi, 1/q, b_i, a_i). \end{aligned} \tag{20c}$$

D. Series expansions for the final observables

Symmetry considerations impose important constraints on the maps $f(\psi, q, a_i, b_i)$, but to make further progress it is useful to Taylor expand these maps about $\mathbf{a} = \mathbf{b} = 0$.[4] In terms of the spin components $\{a_i, b_i\}$, this spin expansion can be written in the form

$$f = f^{m_1 m_2 m_3 | n_1 n_2 n_3}(\psi, q) a_1^{m_1} a_2^{m_2} a_3^{m_3} b_1^{n_1} b_2^{n_2} b_3^{n_3}, \tag{21}$$

where separate summations over the 6 different indices $\{m_1, m_2, m_3, n_1, n_2, n_3\}$ from 0 to ∞ are implied. Note that the expansion coefficients $f^{m_1 m_2 m_3 | n_1 n_2 n_3}$ are now independent of a_i and b_i, but still depend on ψ and q. Naive counting suggests that the number of terms in these expansions should grow rapidly with increasing order in the initial spins (1 zeroth-order term, 6 first-order terms, 21 - second-order terms, and so on). However, the transformation requirements imposed by P and X significantly reduce the number of terms that actually appear.

Under a parity transformation P, the quantities $\{a_1, a_2, b_1, b_2\}$ change sign, implying that individual terms in the expansion are multiplied by $(-1)^\gamma$, where we have defined

$$\gamma \equiv m_1 + m_2 + n_1 + n_2. \tag{22}$$

Equation (11) therefore implies the *parity constraint*:

$$f^{m_1 m_2 m_3 | n_1 n_2 n_3}(q) = (\pm)_P (-1)^\gamma f^{m_1 m_2 m_3 | n_1 n_2 n_3}(q). \tag{23}$$

This may be restated as the *parity rule*:

(i) *Only terms with even (odd) γ can appear in the spin expansion of a (pseudo)scalar f.*

Additionally, if we expand both sides of Eq. (17) and equate terms with the same dependence on the initial spin components, we obtain the *exchange constraint*:

$$f^{m_1 m_2 m_3 | n_1 n_2 n_3}(\psi, q) = (\pm)_{PX} f^{n_1 n_2 n_3 | m_1 m_2 m_3}(\psi, 1/q). \tag{24}$$

Let us again illustrate these results by applying them to the final quantities $f \in \{m, k_i, s_i\}$. We start by writing the expansion as

$$m = m^{m_1 m_2 m_3 | n_1 n_2 n_3}(q, \psi) a_1^{m_1} a_2^{m_2} a_3^{m_3} b_1^{n_1} b_2^{n_2} b_3^{n_3}, \tag{25a}$$

$$\begin{aligned} k_1 &= k_1{}^{m_1 m_2 m_3 | n_1 n_2 n_3}(q, \psi) a_1^{m_1} a_2^{m_2} a_3^{m_3} b_1^{n_1} b_2^{n_2} b_3^{n_3},\\ k_2 &= k_2{}^{m_1 m_2 m_3 | n_1 n_2 n_3}(q, \psi) a_1^{m_1} a_2^{m_2} a_3^{m_3} b_1^{n_1} b_2^{n_2} b_3^{n_3},\\ k_3 &= k_3{}^{m_1 m_2 m_3 | n_1 n_2 n_3}(q, \psi) a_1^{m_1} a_2^{m_2} a_3^{m_3} b_1^{n_1} b_2^{n_2} b_3^{n_3}, \end{aligned} \tag{25b}$$

$$\begin{aligned} s_1 &= s_1{}^{m_1 m_2 m_3 | n_1 n_2 n_3}(q, \psi) a_1^{m_1} a_2^{m_2} a_3^{m_3} b_1^{n_1} b_2^{n_2} b_3^{n_3},\\ s_2 &= s_2{}^{m_1 m_2 m_3 | n_1 n_2 n_3}(q, \psi) a_1^{m_1} a_2^{m_2} a_3^{m_3} b_1^{n_1} b_2^{n_2} b_3^{n_3},\\ s_3 &= s_3{}^{m_1 m_2 m_3 | n_1 n_2 n_3}(q, \psi) a_1^{m_1} a_2^{m_2} a_3^{m_3} b_1^{n_1} b_2^{n_2} b_3^{n_3}. \end{aligned} \tag{25c}$$

The parity constraint, (11) or (23), implies that only terms with the correct parity (even γ) can appear in the expansions of the scalar quantities $\{m, k_1, k_2, s_3\}$. Terms with the wrong parity (odd γ) must vanish. Conversely, only terms with *odd* γ have the correct parity to appear in the expansions of the pseudoscalar quantities $\{s_1, s_2, k_3\}$; terms with wrong parity (even γ) must vanish.

The exchange constraint, (17) or (24), implies that the remaining coefficients must satisfy the following constraints:

[4] In performing this Taylor expansion we assume that the map $f(\psi, q, a_i, b_i)$ is analytic in the neighborhood of $\mathbf{a} = \mathbf{b} = 0$. While recent work by Pretorius and Khurana [45] suggests that certain finely tuned eccentric orbits can be exponentially sensitive to initial conditions, stable circular orbits of nonspinning BBHs should remain circular until the final plunge and merger.

$$m^{m_1m_2m_3|n_1n_2n_3}(q) = +m^{n_1n_2n_3|m_1m_2m_3}(1/q), \tag{26a}$$

$$\begin{aligned} k_1^{m_1m_2m_3|n_1n_2n_3}(q) &= -k_1^{n_1n_2n_3|m_1m_2m_3}(1/q), \\ k_2^{m_1m_2m_3|n_1n_2n_3}(q) &= -k_2^{n_1n_2n_3|m_1m_2m_3}(1/q), \\ k_3^{m_1m_2m_3|n_1n_2n_3}(q) &= -k_3^{n_1n_2n_3|m_1m_2m_3}(1/q), \end{aligned} \tag{26b}$$

$$\begin{aligned} s_1^{m_1m_2m_3|n_1n_2n_3}(q) &= +s_1^{n_1n_2n_3|m_1m_2m_3}(1/q), \\ s_2^{m_1m_2m_3|n_1n_2n_3}(q) &= +s_2^{n_1n_2n_3|m_1m_2m_3}(1/q), \\ s_3^{m_1m_2m_3|n_1n_2n_3}(q) &= +s_3^{n_1n_2n_3|m_1m_2m_3}(1/q). \end{aligned} \tag{26c}$$

where, for brevity, we have not displayed the ψ dependence on each side.

Note that the exchange constraint (24) imposes duality relations between coefficients at q and $1/q$. Without loss of generality, we can focus on the region of initial parameter space with $0 \le q \le 1$, since spin expansions in the region with $1 < q < \infty$ may simply be obtained via the duality relations (24) or (26).

In the equal-mass case, $q = 1 = 1/q$, so the duality relations directly relate previously independent coefficients. In particular, these relations require the kick-velocity coefficients $k_i^{m_1m_2m_3|n_1n_2n_3}$ with $\{m_1, m_2, m_3\} = \{n_1, n_2, n_3\}$ to vanish for $q = 1$ since the components k_i have $(\pm)_{PX} = -1$. This result is consistent with the famous kick formula of Fitchett [53], who was one of the first to calculate the gravitational-wave kick resulting from the merger of nonspinning BBHs in the Newtonian approximation. In his honor, we would like to name the nonspinning kick coefficients $k_i^{000|000}$ "the coeFitchetts."

III. EXACT RESULTS AND SPECIAL CONFIGURATIONS

In this section, we will highlight several *exact* results which follow from the symmetry considerations developed in the previous section. Since they are exact, these predictions may be useful for testing numerical codes which compute BBH mergers numerically.

To derive and summarize the results, it is helpful to think about the operations P and X as elements of a discrete group G of operators acting on binary systems $\mathcal{S}$. This approach conveniently generalizes to include other discrete symmetries like charge conjugation C.[5,6] The three operators P, X, and C all square to unity and commute:

[5] Charge conjugation C is an exact symmetry of classical general relativity and electromagnetism. Under C, the charge Q of a black hole changes sign, $Q \to -Q$.

[6] Though black hole charge is expected to be negligible in astrophysical contexts (and certainly much smaller than the Kerr-Newman bound), it could be important in microphysical contexts—for example if TeV-scale quantum gravity leads to black-hole production in high-energy accelerators, such as the Large Hadron Collider, soon to begin operation at CERN [54].

TABLE II. Transformations of the initial and final observables listed in the first column under the group of operations G formed from parity P, exchange X, and charge conjugation C and listed in the first row.

	P	X	PX	C	PC	XC	PXC
q	q	$1/q$	$1/q$	q	q	$1/q$	$1/q$
a_1	$-a_1$	$-b_1$	$+b_1$	$+a_1$	$-a_1$	$-b_1$	$+b_1$
a_2	$-a_2$	$-b_2$	$+b_2$	$+a_2$	$-a_2$	$-b_2$	$+b_2$
a_3	$+a_3$	$+b_3$	$+b_3$	$+a_3$	$+a_3$	$+b_3$	$+b_3$
b_1	$-b_1$	$-a_1$	$+a_1$	$+b_1$	$-b_1$	$-a_1$	$+a_1$
b_2	$-b_2$	$-a_2$	$+a_2$	$+b_2$	$-b_2$	$-a_2$	$+a_2$
b_3	$+b_3$	$+a_3$	$+a_3$	$+b_3$	$+b_3$	$+a_3$	$+a_3$
Q_a	$+Q_a$	$+Q_b$	$+Q_b$	$-Q_a$	$-Q_a$	$-Q_b$	$-Q_b$
Q_b	$+Q_b$	$+Q_a$	$+Q_a$	$-Q_b$	$-Q_b$	$-Q_a$	$-Q_a$
m	$+m$	$+m$	$+m$	$+m$	$+m$	$+m$	$+m$
k_1	$+k_1$	$-k_1$	$-k_1$	$+k_1$	$+k_1$	$-k_1$	$-k_1$
k_2	$+k_2$	$-k_2$	$-k_2$	$+k_2$	$+k_2$	$-k_2$	$-k_2$
k_3	$-k_3$	$+k_3$	$-k_3$	$+k_3$	$-k_3$	$+k_3$	$-k_3$
s_1	$-s_1$	$-s_1$	$+s_1$	$+s_1$	$-s_1$	$-s_1$	$+s_1$
s_2	$-s_2$	$-s_2$	$+s_2$	$+s_2$	$-s_2$	$-s_2$	$+s_2$
s_3	$+s_3$	$+s_3$	$+s_3$	$+s_3$	$+s_3$	$+s_3$	$+s_3$
Q_f	$+Q_f$	$+Q_f$	$+Q_f$	$-Q_f$	$-Q_f$	$-Q_f$	$-Q_f$

$$\begin{gathered} P^2 = X^2 = C^2 = 1, \\ [P, X] = [P, C] = [X, C] = 0, \end{gathered} \tag{27}$$

so they generate the Abelian group $G = \mathbb{Z}_2 \times \mathbb{Z}_2 \times \mathbb{Z}_2$, with eight elements[7]:

$$G \equiv \{1, P, X, PX, C, PC, XC, PXC\}. \tag{28}$$

The nontrivial elements of this group transform the initial and final quantities in a BBH merger as summarized in Table II.

Each column in Table II (beyond the first) is identified with an operator $g \in G$, and establishes a relationship between two *physically distinct* BBH systems $\mathcal{S}$ and $\mathcal{S}'$ related by $\mathcal{S}' = g\mathcal{S}$, $\mathcal{S} = g\mathcal{S}'$. For example, the second column (P) relates *any* system $\mathcal{S}$ with initial spin components $\{a_i, b_i\}$ to a second system $\mathcal{S}'$ with initial spins

$$\begin{aligned} \{a_1', a_2', a_3'\} &= \{-a_1, -a_2, +a_3\}, \\ \{b_1', b_2', b_3'\} &= \{-b_1, -b_2, +b_3\}. \end{aligned} \tag{29}$$

The final quantities for the system $\mathcal{S}'$ will be given in terms of those for $\mathcal{S}$ by

[7] Time reversal T is another exact symmetry of classical general relativity and electromagnetism. One might hope that we could use T to impose further constraints on binary black hole merger, but unfortunately we cannot. Black hole merger is inherently a dissipative process; we are interested in black holes that emit gravitational waves and inspiral—not those which absorb gravitational waves and outspiral.

TABLE III. Special initial configurations (''Input''), and the corresponding predictions for the final state (''Output'').

	Input	Output
P	$a_1 = a_2 = b_1 = b_2 = 0$	$s_1 = s_2 = k_3 = 0$
X	$(a_1, a_2) = -(b_1, b_2),\ \ a_3 = b_3,\ \ q = 1,\ \ Q_a = Q_b$	$k_1 = k_2 = s_1 = s_2 = 0$
PX	$(a_1, a_2, a_3) = (b_1, b_2, b_3),\ \ q = 1,\ \ Q_a = Q_b$	$k_1 = k_2 = k_3 = 0$
C	$Q_a = Q_b = 0$	$Q_f = 0$
PC	$a_1 = a_2 = b_1 = b_2 = 0,\ \ Q_a = Q_b = 0$	$s_1 = s_2 = k_3 = Q_f = 0$
XC	$(a_1, a_2) = -(b_1, b_2),\ \ a_3 = b_3,\ \ q = 1,\ \ Q_a = -Q_b$	$k_1 = k_2 = s_1 = s_2 = Q_f = 0$
PXC	$(a_1, a_2, a_3) = (b_1, b_2, b_3),\ \ q = 1,\ \ Q_a = -Q_b$	$k_1 = k_2 = k_3 = Q_f = 0$

$$\begin{aligned} \{k_1', k_2', k_3'\} &= \{+k_1, +k_2, -k_3\}, \\ \{s_1', s_2', s_3'\} &= \{-s_1, -s_2, +s_3\}, \\ \{m', Q_f'\} &= \{m, Q_f\}. \end{aligned} \tag{30}$$

Some of the 7 predicted relationships represented by the 7 columns of Table II may be useful to numerical relativists for identifying errors in their numerical codes that fail to respect the given symmetries. For example, P demands that simulations of the systems $\mathcal{S}$ and $\mathcal{S}'$ must yield final quantities that are related by Eq. (30). Any deviations from this relationship would reveal systematic errors in the simulations that need to be corrected.

Each nontrivial element $g \in G$ not only establishes a dual system $\mathcal{S}' = g\mathcal{S}$ for *all* BBH systems $\mathcal{S}$, but also defines a ''special'' configuration $\mathcal{S}_g$ that is its *own* dual, i.e. $g\mathcal{S}_g = \mathcal{S}_g$. Since the initial state is invariant under g, the final state must also be invariant, so we can conclude that any final quantity f that is *not* invariant under g must vanish. For example, consider the second column (P) in Table II. We see that, if the initial configuration satisfies $a_1 = a_2 = b_1 = b_2 = 0$, then a parity transformation P leaves this initial configuration invariant. Therefore, we can conclude that the corresponding final state must satisfy $s_1 = s_2 = k_3 = 0$, since these 3 quantities are *not* invariant under P. Similarly, from each of the 7 columns in Table II, we can read off a special initial configuration, and the corresponding predictions for the final state of the system. These 7 special configurations, and their consequences, are summarized in Table III.

IV. TESTING OUR EXPANSIONS WITH EXISTING SIMULATIONS

Although the previous section's exact results are interesting, the real power of the spin expansion is in the much larger set of *approximate* predictions it makes for generic spin configurations.

Currently, published simulations of BBH mergers can be subdivided into 5 different classes of initial spin configurations. For each of these classes, we compare in detail the predictions of the spin expansion with existing numerical results. As we shall see, the spin expansion makes new and successful predictions in each case, and provides a simple and systematic way of *deriving* features of existing simulations that were previously opaque.

Since rigorous systematic errors are not yet available for many of the simulated data sets analyzed in this section, our analysis of these simulations will by necessity be correspondingly nonrigorous. In particular, we will use the following rather heuristic procedure. For each data set, we compute the χ^2 per degree of freedom (χ^2/d.o.f.). We do *not* attribute meaning to the overall value of the χ^2/d.o.f. (since, in many cases, we have had to guess error bars for the simulated data). However, if including a new term predicted by the spin expansion leads to a large *fractional* reduction in the χ^2/d.o.f., we interpret this reduction as admittedly nonrigorous evidence for this new term. Note that an overall rescaling of the error bars will *not* lead to a fractional reduction in the χ^2/d.o.f., so the conclusions in this section should be largely insensitive to our estimates for the error bars.

In any case, statistical rigor is *not* the point of this section. Our goal is to illustrate our formalism through a few worked examples, to demonstrate its power to explain currently available simulations, and to make several predictions for future simulations. It will usually be clear (by eye) that our leading-order and next-to-leading-order formulas provide a good explanation of the basic qualitative features seen in the simulated data thus far.

We have summarized our use of simulations in Appendix A, where we also explain our estimates for the corresponding error bars—which are often just crude guesses. The crudeness of these guesses sometimes leads to impossibly small χ^2/d.o.f. for our fits. This is primarily because genuine errors in the simulations are *systematic*, whereas published works (and our own analysis) treat these errors as *statistical*. Systematic errors that preserve the symmetries of the configuration will be well fit by our expansions, regardless of their size, albeit with erroneous numerical values for the best-fit coefficients.

In this section, we will often encounter 3-component quantities (x_1, x_2, x_3) where we wish to treat the ''1'' and ''2'' components together, without the ''3'' component.

Thus, it is convenient to introduce the notation

$$\mathbf{x}_\perp = (x_1, x_2) \tag{31}$$

as these components are *perpendicular* to the orbital angular momentum vector. So, for example, $\mathbf{a}_\perp = (a_1, a_2)$, $\mathbf{k}_\perp = (k_1, k_2)$, and $\mathbf{k}_\perp^{001|000} = (k_1^{001|000}, k_2^{001|000})$. From a notational standpoint, $\mathbf{x}_\perp$ acts like a "2-vector" in the sense that

$$|\mathbf{x}_\perp| \equiv \sqrt{x_1^2 + x_2^2}, \qquad \mathbf{x}_\perp \cdot \mathbf{y}_\perp = x_1 y_1 + x_2 y_2. \tag{32}$$

A. Case 1: Nonprecessing spins ($q = 1$ and $\mathbf{a} \propto \mathbf{b} \propto \mathbf{e}^{(3)}$)

First consider the case in which the black holes have equal mass ($q = 1$), and both spins are aligned (or anti-aligned) with the orbital angular momentum:

$$\begin{pmatrix} a_1 \\ a_2 \\ a_3 \end{pmatrix} = \begin{pmatrix} 0 \\ 0 \\ a_3 \end{pmatrix}, \qquad \begin{pmatrix} b_1 \\ b_2 \\ b_3 \end{pmatrix} = \begin{pmatrix} 0 \\ 0 \\ b_3 \end{pmatrix}. \tag{33}$$

This corresponds to the special configuration identified with the operator P in the previous section, for which k_3 and $\mathbf{s}_\perp$ exactly vanish. What about *nonvanishing* observables like $\mathbf{k}_\perp$, s_3, and m?

The zeroth-order terms in the s_3 and m expansions are nonvanishing, and physically correspond to the spin and mass of the final black hole produced in the merger of two nonspinning holes A and B. However, exchange X requires the zeroth-order term in the $\mathbf{k}_\perp$ expansion (the "coeFitchett" $\mathbf{k}_\perp^{000|000}$) to vanish, as discussed in Sec. II D. To capture the leading-order (LO), next-to-leading-order (NLO), and next-to-next-to-leading-order (NNLO) behavior, we therefore expand s_3 and m to second order in the initial spins and $\mathbf{k}_\perp$ to third order.

Using the parity and exchange constraints, (23) and (24), to equate or eliminate coefficients, our expansions (25) for this configuration become

$$\begin{aligned}\mathbf{k}_\perp &= \mathbf{k}_\perp^{001|000}(a_3 - b_3) + \mathbf{k}_\perp^{002|000}(a_3^2 - b_3^2) \\ &\quad + \mathbf{k}_\perp^{003|000}(a_3^3 - b_3^3) + \mathbf{k}_\perp^{002|001}(a_3^2 b_3 - b_3^2 a_3),\end{aligned} \tag{34a}$$

$$\begin{aligned}s_3 &= s_3{}^{000|000} + s_3{}^{001|000}(a_3 + b_3) \\ &\quad + s_3{}^{002|000}(a_3^2 + b_3^2) + s_3{}^{001|001} a_3 b_3,\end{aligned} \tag{34b}$$

$$\begin{aligned}m &= m^{000|000} + m^{001|000}(a_3 + b_3) \\ &\quad + m^{002|000}(a_3^2 + b_3^2) + m^{001|001} a_3 b_3.\end{aligned} \tag{34c}$$

Unfortunately for us, currently published simulations only report the magnitude $|\mathbf{k}_\perp| = \sqrt{k_1^2 + k_2^2}$, not the individual components k_1 and k_2. Taking the magnitude of the expansion (34a) for $\mathbf{k}_\perp$ and Taylor expanding to third order in the initial spins yields

$$\begin{aligned}|\mathbf{k}_\perp| &= |\mathbf{k}_\perp^{001|000}||a_3 - b_3| \\ &\quad \times [1 + A(a_3 + b_3) + B(a_3^2 + b_3^2) + C a_3 b_3].\end{aligned} \tag{35}$$

For convenience, we have introduced new coefficients A, B, and C, which may be expressed in terms of the original expansion coefficients $\mathbf{k}_\perp^{m_1 m_2 m_3|n_1 n_2 n_3}$. These expressions are given in Appendix B 1.

It is interesting to note that, although $|\mathbf{k}_\perp|$ is *even* under both P and X (just like s_3 and m), its expansion (35) is different from the s_3 and m expansions (34b) and (34c). This is a reflection of the fact that, although $|\mathbf{k}_\perp|$ has the same transformation properties as s_3 and m, it is a composite quantity constructed from more "fundamental" quantities (k_1 and k_2) with different transformation properties. Looking more closely, we notice that the expression inside square brackets in Eq. (35) bears a close formal resemblance to the expansions (34b) and (34c): there is a constant term at LO, a term proportional to $(a_3 + b_3)$ at NLO, and two terms proportional to $(a_3^2 + b_3^2)$ and $a_3 b_3$ at NNLO. The compositeness of $|\mathbf{k}_\perp|$ manifests itself through the overall factor of $|a_3 - b_3|$ in front of the square brackets in (35).

Equations (34b), (34c), and (35) make detailed quantitative predictions for the final kicks, spins, and masses—let us see how they stack up against actual simulations.

Many groups have published results from the simulations of binary mergers with initial spins aligned or anti-aligned with the angular momentum direction $\mathbf{e}^{(3)}$ [2,11,13,14,16,55]. While all groups begin their simulations with the binary on a quasicircular orbit, they make different choices for the initial dimensionless orbital separation $r/(M_a + M_b)$. As explained in Sec. II, our expansion coefficients (25) are defined at a fixed value of the inspiral parameter ψ, which in this case is the dimensionless orbital separation $r/(M_a + M_b)$. Connecting simulations performed at different values of ψ will in general require careful use of post-Newtonian approximations as discussed in a forthcoming paper. However, for the special case considered here (where $\mathbf{a} \propto \mathbf{b} \propto \mathbf{e}^{(3)}$), the initial spins will not precess and their projection onto the orthonormal triad $\{\mathbf{e}^{(1)}, \mathbf{e}^{(2)}, \mathbf{e}^{(3)}\}$ will not vary with orbital phase. As such, it is possible in principle to jointly fit all the simulations even though they do not all correspond to the same initial separation. In practice, there are systematic differences between numerical codes[8] which make a combined fit to all existing simulations unreliable. In Appendix A 1,

[8]For example, Pollney *et al.* [13] discuss the necessity of properly choosing an integration constant corresponding to the linear momentum acquired before the simulations begins. Rezzolla *et al.* [14] suggest that this integration constant may be responsible for the discrepancy between their results and those of [11].

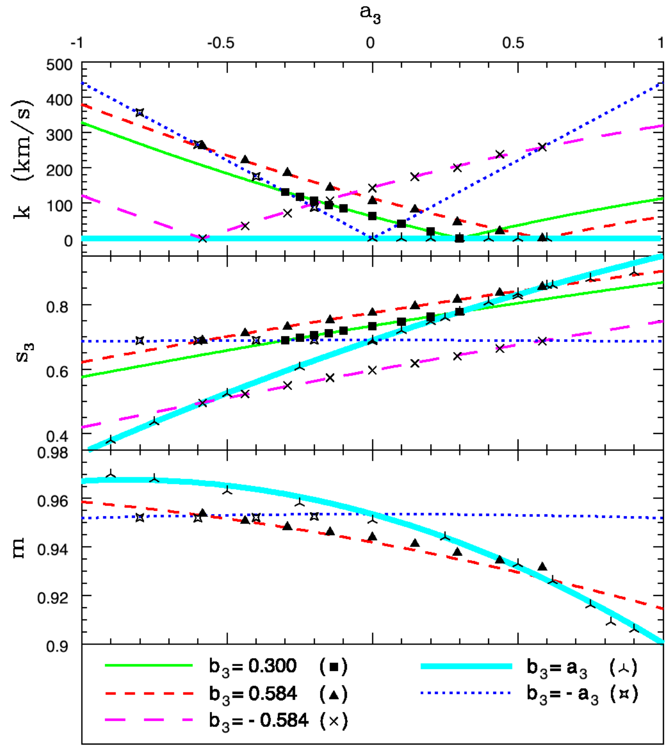

FIG. 2 (color online). Case 1 best-fit curves. The top, center, and bottom panels show, respectively, the kick velocity $|\mathbf{k}_\perp|$, dimensionless spin s_3, and dimensionless mass m of the final black hole. The data points appearing in each panel are described in Appendix A 1. The curves in the top, center, and bottom panels correspond, respectively, to Eqs. (34b), (34c), and (35), with the coefficients given in Table IV. Each curve has a fixed value of b_3 given by the legend at the bottom of the figure, with a_3 varying along the abscissa. For presentation purposes, we have switched a_3 and b_3 for points on the magenta (long-dashed) curve; this exchange does not affect the values of $|\mathbf{k}_\perp|$ and s_3.

we describe our choice of simulations to test Eqs. (34b), (34c), and (35).

First consider the final kick $|\mathbf{k}_\perp|$. At leading order, Eq. (35) predicts that $|\mathbf{k}_\perp|$ should be proportional to $|a_3 - b_3|$; this approximately linear behavior has been noticed in simulations in several previous papers [8,11,13]. At next-to-leading order, Eq. (35) predicts that $|\mathbf{k}_\perp|$ should receive a small additive correction proportional to $|a_3 - b_3|(a_3 + b_3)$. This prediction is well supported by the simulations in the following sense. When we fit the 28 simulations in [14] with nonzero values for $|\mathbf{k}_\perp|$ to the leading-order term in Eq. (35), there is only one fitting parameter (namely, the magnitude $|\mathbf{k}_\perp^{001|000}|$), and the fit is rather poor $\chi^2/\text{d.o.f.} = 38.2/(28-1) \approx 1.4$. Then, when we include the next-to-leading-order term, there is one more fitting parameter (namely, A), and the fit improves dramatically: $\chi^2/\text{d.o.f.} = 5.14/(28-2) \approx 0.2$. We interpret this significant drop in the $\chi^2/\text{d.o.f.}$ as strong evidence for the second-order term in Eq. (35).[9] This NLO fit, with only two fitting parameters ($|\mathbf{k}_\perp|$ and A), is displayed in the top panel of Fig. 2.

TABLE IV. Case 1 best-fit parameters, from fitting Eqs. (34b), (34c), and (35) to the final kicks, spins, and masses of the simulations described in Appendix A 1. These fits are displayed in Fig. 2.

Data set	Best-fit coefficients
$\lvert\mathbf{k}_\perp\rvert$ (28 simulations)	$\lvert\mathbf{k}_\perp^{001\|000}\rvert \approx 221$ km/s
	$A \approx -0.205$
	$B \approx -0.091$
	$C \approx -0.201$
s_3 (48 simulations)	$s_3^{000\|000} \approx 0.6893$
	$s_3^{001\|000} \approx 0.1524$
	$s_3^{001\|001} \approx -0.0195$
	$s_3^{002\|000} \approx -0.0121$
m (24 simulations)	$m^{000\|000} \approx 0.9530$
	$m^{001\|000} \approx -0.0167$
	$m^{001\|001} \approx -0.0083$
	$m^{002\|000} \approx -0.0052$

Is there also evidence for the NNLO terms in Eq. (35)? When we include these final two terms, there are two more fitting parameters (B and C), and the fit again improves significantly: $\chi^2/\text{d.o.f.} = 2.2/(28-4) \approx 0.09$. Our best-fit values for the 4fitting parameters in Eq. (35) are shown in Table IV.

Next consider the final spin s_3 and the final mass m. It is convenient to treat these two quantities in parallel, since their expansions (34b) and (34c) are formally identical to each other. Equations (34b) and (34c) predict that at zeroth order the final spin s_3 and final mass m should be equal, respectively, to the final spin $s_3^{000|000}$ and final mass $m^{000|000}$ from the merger of two *nonspinning* black holes. At first order, there should be a linear correction proportional to $(a_3 + b_3)$, and at second order there should be two corrections: one proportional to $a_3 b_3$, and the other proportional to $(a_3^2 + b_3^2)$.[10]

These predictions are again supported by the simulations. First consider s_3. By itself, the leading-order term $s_3^{000|000}$ gives a poor fit $[\chi^2/\text{d.o.f.} = 3661/(48-1) = 77.9]$ to the 48 simulations of [14,16]. When we include the NLO term, $s_3^{001|000}(a_3 + b_3)$, the fit improves dramati-

[9]Pollney *et al.* [13] also noted a significant deviation from linearity in the kick magnitudes for initially (anti)aligned spins, although their guess for the correction term differs from that derived via our formalism. Rezzolla *et al.* [14] arrived at the *same* second-order fitting formula as we did using similar considerations; our parameters $|\mathbf{k}_\perp^{001|000}|$ and A correspond to $|c_1|$ and c_2/c_1 in their notation.

[10]Rezzolla *et al.* [14] argued that BBHs with equal and opposite spins ($a_3 = -b_3$) should behave as if they were nonspinning, so that only a single term $p_2(a_3 + b_3)^2$ should appear at second order. According to this conjecture our coefficients should be related as $s_3^{002|000} = 1/2 s_3^{001|001} = p_2$.

cally [χ^2/d.o.f. $= 16.8/(48-2) = 0.366$]. Finally, when we add the NNLO terms, $s_3^{002|000}(a_3^2+b_3^2)$ and $s_3^{001|001}a_3b_3$, the fit is even better [χ^2/d.o.f. $= 0.0386$]. The fit to m using Eq. (34c) is closely analogous: the zeroth-order fit is again lousy [χ^2/d.o.f. $= 436/(24-1) = 19.0$]; the first-order fit is much improved [χ^2/d.o.f $= 46.8/(24-2) = 2.13$]; and the second-order fit is better still [χ^2/d.o.f $= 5.30/(24-4) = 0.265$]. Thus, in both the s_3 and m data sets, we have clear evidence for both NLO and NNLO corrections.[11] Our best-fit parameters are shown in Table IV, and the corresponding fits to s_3 and m are plotted in Fig. 2, in the middle and bottom panels, respectively.

Though we have used numerical simulations to calibrate the values of the coefficients in our spin expansions, physical intuition provides some insight into these values. Test particles with orbital angular mometum aligned with the spin of a Kerr black hole have innermost stable circular orbits (ISCOs) with smaller radii, and therefore emit more gravitational radiation before merger. Similar behavior has been observed for comparable-mass black holes in numerical simulations [15]. This suggests, as we have indeed found by comparing to simulations, that the coefficient $m^{001|000}$ should be negative: more orbits imply more energy carried away in gravitational waves and a smaller final mass. The impact on the final spin is more ambiguous; aligned BBHs should convey more spin angular momentum to the final black hole, but less orbital angular momentum because of their smaller ISCOs. Since $s_3^{001|000}$ is positive we conclude that the former effect dominates over the latter though its comparatively small value evidences significant cancellation.

B. Case 2: "Superkick" configuration ($q = 1$, $\mathbf{a} = -\mathbf{b}$, $a_3 = b_3 = 0$)

We next consider the case in which the black holes have equal mass ($q = 1$) and equal and opposite spins lying in the orbital plane:

$$\begin{pmatrix} a_1 \\ a_2 \\ a_3 \end{pmatrix} = \begin{pmatrix} +a\cos\phi \\ +a\sin\phi \\ 0 \end{pmatrix}, \qquad \begin{pmatrix} b_1 \\ b_2 \\ b_3 \end{pmatrix} = \begin{pmatrix} -a\cos\phi \\ -a\sin\phi \\ 0 \end{pmatrix}. \tag{36}$$

As shown in Sec. III (Table III), this is an example of the special configuration associated with the exchange operator X, for which $\mathbf{k}_\perp$ and $\mathbf{s}_\perp$ exactly vanish. What about the nonvanishing quantities k_3, s_3, and m?

[11] The final spins and masses are equally well fit by a single second-order term proportional to $(a_3+b_3)^2$ as suggested by Rezzolla *et al.* [14]. Though post-Newtonian approximations may suggest that the spin-spin term proportional to a_3b_3 comes in at higher order, we restrict ourselves to what can be asserted purely on the basis of our formalism.

The superkick initial spin configuration (36) is parametrized by only two numbers (a and ϕ), instead of six (a_i and b_i). As a result, when we substitute Eq. (36) into the original spin expansions of Eq. (25), many of the terms become degenerate with one another. It is convenient to eliminate this degeneracy by collecting all terms with the same dependence on a and ϕ. Then the spin expansion takes the form

$$f = \sum_{i=0}^{\infty}\sum_{j=0}^{i}[{}^s f^{(i,j)} a^i \sin(j\phi) + {}^c f^{(i,j)} a^i \cos(j\phi)], \tag{37a}$$

where f represents one of the nonvanishing final observables (e.g. k_3, s_3, or m). The coefficients ${}^s f^{(i,j)}$ and ${}^c f^{(i,j)}$ are finite linear combinations of the original spin-expansion coefficients $f^{m_1m_2m_3|n_1n_2n_3}$. These linear combinations can be derived explicitly by equating the two expansions (25) and (37a) term by term; the first few combinations are provided in Appendix B 2.

For situations in which ϕ varies while a remains fixed, we should go one step beyond Eq. (37a) by collecting all terms with the same ϕ dependence. Then Eq. (37a) is rewritten in the form

$$f = \sum_{j=0}^{\infty}[{}^s f^{(j)} \sin(j\phi) + {}^c f^{(j)} \cos(j\phi)], \tag{37b}$$

where we have defined the coefficients

$${}^s f^{(j)} \equiv \sum_{i=j}^{\infty} {}^s f^{(i,j)} a^i, \qquad {}^c f^{(j)} \equiv \sum_{i=j}^{\infty} {}^c f^{(i,j)} a^i. \tag{38}$$

We stress that Eq. (37a) is the *same* series as Eq. (37b). The first form (37a) is appropriate for situations where a and ϕ both vary, whereas the second form (37b) is appropriate for situations where ϕ varies but a does not.

Symmetry considerations further restrict the terms that can appear in the expansions (37). Applying parity P to the initial configuration (36) is equivalent to the transformation $\phi \to \phi + \pi$ which sends $\{\sin(j\phi), \cos(j\phi)\} \to \{(-1)^j \sin(j\phi), (-1)^j \cos(j\phi)\}$. It follows that

(i) *in the superkick configuration* (36), *only terms with even (odd) i and j can appear in the expansions* (37) *for a scalar (pseudoscalar) quantity f.*

Since the superkick initial spin configuration (36) is invariant under X, an exchange transformation does not yield any further constraints.

These simple considerations lead to detailed quantitative predictions. To illustrate this point, let us start by displaying some of the leading terms in the expansions (37a) for the nonvanishing observables k_3, s_3, and m:

$$\begin{aligned} k_3 = {} & [{}^s k_3^{(1,1)} a^1 + {}^s k_3^{(3,1)} a^3 + \mathcal{O}(a^5)] \sin(\phi) \\ & + [{}^c k_3^{(1,1)} a^1 + {}^c k_3^{(3,1)} a^3 + \mathcal{O}(a^5)] \cos(\phi) \\ & + [{}^s k_3^{(3,3)} a^3 + {}^s k_3^{(5,3)} a^5 + \mathcal{O}(a^7)] \sin(3\phi) \\ & + [{}^c k_3^{(3,3)} a^3 + {}^c k_3^{(5,3)} a^5 + \mathcal{O}(a^7)] \cos(3\phi) + \cdots, \end{aligned} \tag{39a}$$

$$\begin{aligned} s_3 = {} & [{}^c s_3^{(0,0)} a^0 + {}^c s_3^{(2,0)} a^2 + \mathcal{O}(a^4)] \cos(0\phi) \\ & + [{}^s s_3^{(2,2)} a^2 + {}^s s_3^{(4,2)} a^4 + \mathcal{O}(a^6)] \sin(2\phi) \\ & + [{}^c s_3^{(2,2)} a^2 + {}^c s_3^{(4,2)} a^4 + \mathcal{O}(a^6)] \cos(2\phi) + \cdots, \end{aligned} \tag{39b}$$

$$\begin{aligned} m = {} & [{}^c m^{(0,0)} a^0 + {}^c m^{(2,0)} a^2 + \mathcal{O}(a^4)] \cos(0\phi) \\ & + [{}^s m^{(2,2)} a^2 + {}^s m^{(4,2)} a^4 + \mathcal{O}(a^6)] \sin(2\phi) \\ & + [{}^c m^{(2,2)} a^2 + {}^c m^{(4,2)} a^4 + \mathcal{O}(a^6)] \cos(2\phi) + \cdots. \end{aligned} \tag{39c}$$

In these equations, we have explicitly displayed the $\cos(0\phi) = 1$ factors to emphasize the similarity between the $j = 0$ and $j \neq 0$ terms.

First consider the predictions of Eq. (39a) for the kick velocity k_3. The leading-order $[\mathcal{O}(a^1)]$ terms predict that this kick should vary as $\sin(\phi + \text{phase})$ at a fixed value of a, and that the *amplitude* of this sinusoid should scale *linearly* with a. The next-to-leading-order $[\mathcal{O}(a^3)]$ terms predict that this leading $\sin(\phi + \text{phase})$ behavior should receive a small additive correction of the form $\sin(3\phi + \text{phase})$ with amplitude proportional to a^3. Next consider the predictions of Eq. (39b) for the final spin s_3. The leading-order $[\mathcal{O}(a^0)]$ term predicts that the final spin is a constant, independent of both a and ϕ: $s_3 \propto a^0 \cos(0\phi)$. The next-to-leading-order $[\mathcal{O}(a^2)]$ terms predict that the leading $\cos(0\phi)$ behavior should receive a small additive correction of the form $\sin(2\phi + \text{phase})$ with amplitude proportional to a^2. Finally, since Eq. (39c) is formally identical to Eq. (39b), m should behave in the same way as s_3.

We test these predictions using the published simulations of [5,6], with relevant data and errors described in Appendix A 2. Although both papers estimate the final kicks k_3, the simulations in [5] start at a different orbital separation $r/(M_a + M_b)$ from those in [6]. In Sec. IVA, we were able to jointly fit simulations with different initial separations because the relevant spin-expansion coefficients were insensitive to the initial separation. Unfortunately, in the present configuration (36), the relevant expansion coefficients *are* sensitive to the initial separation. As we discuss in a future paper, it should be possible to connect the expansion coefficients at different initial separations using post-Newtonian techniques. For the time being, though, we must perform separate fits for the simulation sets $\{A_i\}$ of [5] and $\{B_i\}$ of [6]. As the initial spin magnitude a is fixed within each data set, we should use the spin expansion in the form (37b). Thus, for the nonvanishing observables k_3, s_3, and m, we have the expressions:

TABLE V. Fits for case 2. The first column lists the coefficients being determined. Kick velocities are in units of km/s while the remaining coefficients are dimensionless. The second column provides the best-fit values for these coefficients when the lowest-order terms are fit to data set A, the simulations of [5]. Expansions for the radiated angular momentum $J_{\rm rad}/M^2$ and energy $\%E_{\rm rad}$ have zeroth-order terms while first order is lowest for k_3. The third column lists best-fit values for next-to-lowest-order fits; this is second order for $J_{\rm rad}/M^2$ and $\%E_{\rm rad}$ and third order for k_3. The fourth and fifth columns list the corresponding values of coefficients for data set B, the simulations of [6]. This data set provides the spin s_3 of the final black hole instead of $J_{\rm rad}/M^2$ and $\%E_{\rm rad}$. The expansion for s_3 has zeroth- and second-order terms.

Data set	A	A	B	B
${}^c k_3^1$	-350	-323	3753	2714
${}^s k_3^1$	1876	1837	-343	-246
${}^c k_3^3$	$\cdots$	-29.4	$\cdots$	-20.8
${}^s k_3^3$	$\cdots$	2.73	$\cdots$	83.5
${}^c(J_{\rm rad}/M^2)^0$	0.2471	0.2471	$\cdots$	$\cdots$
${}^c(J_{\rm rad}/M^2)^2$	$\cdots$	-0.0012	$\cdots$	$\cdots$
${}^s(J_{\rm rad}/M^2)^2$	$\cdots$	-0.0027	$\cdots$	$\cdots$
${}^c s_3^0$	$\cdots$	$\cdots$	0.6895	0.6895
${}^c s_3^2$	$\cdots$	$\cdots$	$\cdots$	-0.0038
${}^s s_3^2$	$\cdots$	$\cdots$	$\cdots$	-0.0021
${}^c(\%E_{\rm rad})^0$	3.587	3.600	$\cdots$	$\cdots$
${}^c(\%E_{\rm rad})^2$	$\cdots$	-0.0301	$\cdots$	$\cdots$
${}^s(\%E_{\rm rad})^2$	$\cdots$	-0.0695	$\cdots$	$\cdots$

$$\begin{aligned} k_3 = {} & {}^s k_3^{(1)} \sin(\phi) + {}^c k_3^{(1)} \cos(\phi) + {}^s k_3^{(3)} \sin(3\phi) \\ & + {}^c k_3^{(3)} \cos(3\phi) + \mathcal{O}(a^5), \end{aligned} \tag{40a}$$

$$s_3 = {}^c s_3^{(0)} + {}^s s_3^{(2)} \sin(2\phi) + {}^c s_3^{(2)} \cos(2\phi) + \mathcal{O}(a^4), \tag{40b}$$

$$m = {}^c m^{(0)} + {}^s m^{(2)} \sin(2\phi) + {}^c m^{(2)} \cos(2\phi) + \mathcal{O}(a^4). \tag{40c}$$

Instead of reporting s_3 and m, Campanelli *et al.* [5] report the percentage of the initial energy carried away by gravitational radiation $\%E_{\rm rad}$ and the dimensionless radiated angular momentum $J_{\rm rad}/M^2$. Since both of these quantities are scalars, with $P = +1$ and $X = +1$, their expansions are exactly analogous to the expansions for m and s_3 in Eqs. (40b) and (40c). The best-fit coefficients from our leading-order and next-to-leading-order fits to these quantities are listed in Table V, and the leading-order fits themselves are displayed in Fig. 3.

First focus on the kick velocity k_3. The top panel in Fig. 3 clearly reveals the $\sin(\phi + \text{phase})$ behavior predicted (at leading order) by the spin expansion, and pre-

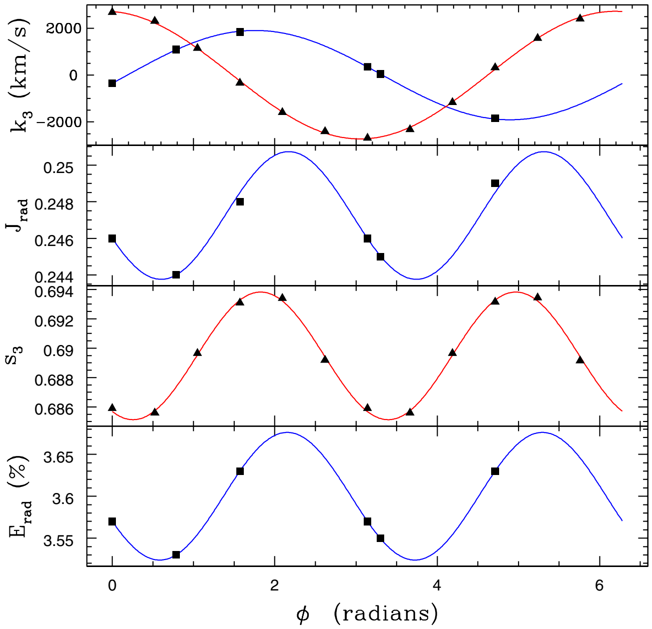

FIG. 3 (color online). Case 2 best-fit curves. Panels from top to bottom show the kick velocity k_3, the radiated angular momentum $J_{\rm rad}$, the final spin s_3, and the percentage of radiated energy $E_{\rm rad}$, all plotted against the angle ϕ between the initial spin $\mathbf{a}$ and $\mathbf{e}^{(1)}$. The blue curves show fits to the square data points taken from [5], while the red curves show fits to the triangle data points of [6]. The curves for k_3 only show the first-order terms in Eq. (40a), while those for $J_{\rm rad}$, s_3, and $E_{\rm rad}$ include all terms up to second order. The χ^2/d.o.f. and best-fit coefficients are listed in Table V.

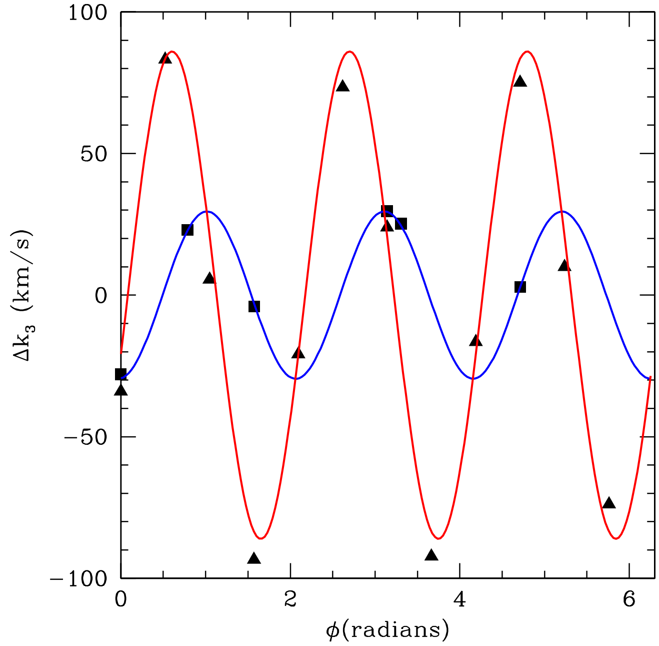

FIG. 4 (color online). The residuals Δk_3 after the first-order terms of Eq. (40a) are subtracted from the simulated final kicks. As in the top panel of Fig. 3, the blue curves show fits to the square data points taken from [5], while the red curves show fits to the triangle data points of [6]. These curves consist of the third-order terms of Eq. (40a) with the coefficients listed in Table V.

viously noted in Eq. (1) of [5] and Eq. (6) of [6]. Although the spin expansion cannot predict the phases of the sine waves in this panel, it predicts that (at leading order) their amplitudes should be proportional to the spin magnitude a. This prediction is also supported by the simulations: the ratio of the best-fit values of $[({}^sk_3^{(1)})^2 + ({}^ck_3^{(1)})^2]^{1/2}$ for the simulations $\{A_i\}$ of [5] and $\{B_i\}$ of [6] is 0.684, not far off from the ratio of their spins $0.515/0.723 = 0.712$.

The *next-to-leading-order* predictions of the spin expansion for k_3 also appear to be confirmed. To see this, we subtract the leading-order $\sin(\phi + \text{phase})$ prediction from the simulated k_3 data, and plot the residuals in Fig. 4. As predicted, these residuals oscillate as $\sin(3\phi + \text{phase})$. Furthermore, the amplitude of this residual oscillation scales as a^3, as predicted. The ratio of the best-fit values of $[({}^ck_3^{(3)})^2 + ({}^sk_3^{(3)})^2]^{1/2}$ for the simulations $\{A_i\}$ and $\{B_i\}$ is 0.343, which is close to the spin ratio cubed, $(0.515/0.723)^3 = 0.361$.

Thus, we have seen that the spin expansion succeeds in reproducing previously observed aspects of the k_3 data, and also in predicting previously unrecognized features.

The remaining three panels in Fig. 3 show observables whose ϕ dependence agrees closely with what we expect for scalars like s_3 and m in Eqs. (40b) and (40c). At zeroth order they are independent of ϕ, while at next-to-leading order the predicted $\sin(2\phi + \text{phase})$ contribution appears.[12] Unfortunately for us, [5,6] chose to publish different observables so we cannot test whether the amplitude of these double-frequency terms really scales like a^2 as predicted. Hopefully, future simulations performed at different values of a will address this question.

C. Case 3: Herrmann *et al.* "B-series" ($q = 1$, $\mathbf{a} = -\mathbf{b}$, $a_2 = b_2 = 0$)

We next consider the "B-series" simulations of Herrmann *et al.* [7]. This configuration consists of equal-mass black holes with equal-magnitude, oppositely directed spins lying in the $(\mathbf{e}^{(1)}, \mathbf{e}^{(3)})$ plane:

[12]Brügmann *et al.* [6] noted a $\sin(2\phi + \text{phase})$ dependence in s_3, but concluded that it might be a nonphysical systematic error, since they could not find a consistent $\sin(\phi + \text{phase})$ contribution (see their Fig. 13, and corresponding discussion). Our formalism explains why the $\sin(\phi + \text{phase})$ term is forbidden, and suggests that the oscillation which they observe is probably a real physical effect, not a systematic error.

$$\begin{pmatrix} a_1 \\ a_2 \\ a_3 \end{pmatrix} = \begin{pmatrix} +a\sin\phi \\ 0 \\ +a\cos\phi \end{pmatrix}, \qquad \begin{pmatrix} b_1 \\ b_2 \\ b_3 \end{pmatrix} = \begin{pmatrix} -a\sin\phi \\ 0 \\ -a\cos\phi \end{pmatrix}. \tag{41}$$

Though this is obviously a highly symmetric configuration, it is not one of the special configurations derived in Sec. III and therefore has nonvanishing values for all of the final observables $f \in \{m, \mathbf{k}_\perp, k_3, \mathbf{s}_\perp, s_3\}$. As in case 2, the initial spin configuration (41) is parametrized by two numbers (a and ϕ) instead of six $\{a_i, b_i\}$, so that the original spin expansions (25) become highly degenerate. Therefore, just as in case 2, we should remove these degeneracies by collecting terms with the same dependence on a and ϕ, and rewriting the expansion in the form (37a), or equivalently (37b) and (38). For convenience, Appendix B 3 provides explicit expressions for the "new" coefficients $\{{}^c f^{(i,j)}, {}^s f^{(i,j)}\}$ in terms of the original spin-expansion coefficients $f^{m_1 m_2 m_3 | n_1 n_2 n_3}$, up to third order in a.

Since the B-series configuration (41) has different symmetries from the superkick configuration (36), there are different rules governing which terms appear in the expansions (37) for each observable. We can discover these rules as follows. Applying a parity transformation P to the initial configuration (41) is equivalent to sending $\phi \to -\phi$, and hence $\{\sin(j\phi), \cos(j\phi)\} \to \{-\sin(j\phi), \cos(j\phi)\}$. From this we infer that

(i) *in the B-series configuration* (41), *only cosine (sine) terms can appear in the expansions* (37) *for a scalar (pseudoscalar) quantity* f.

Applying a combined parity and exchange transformation PX to the initial configuration (41) is equivalent to the transformation $\phi \to \phi + \pi$, and therefore $\{\sin(j\phi), \cos(j\phi)\} \to \{(-1)^j \sin(j\phi), (-1)^j \cos(j\phi)\}$. We thus infer that

(i) *in the B-series configuration* (41), *only terms with even (odd) i and j can appear in the expansions* (37) *for a quantity* f *that is even (odd) under* PX.

From these simple considerations, a host of interesting predictions follow.[13] To illustrate this point, consider the expansions for $f \in \{k_i, s_i, m\}$:

$$\mathbf{k}_\perp = [{}^c\mathbf{k}_\perp^{(1,1)} a^1 + {}^c\mathbf{k}_\perp^{(3,1)} a^3 + \mathcal{O}(a^5)]\cos(\phi) + [{}^c\mathbf{k}_\perp^{(3,3)} a^3 + {}^c\mathbf{k}_\perp^{(5,3)} a^5 + \mathcal{O}(a^7)]\cos(3\phi) + \cdots, \tag{42a}$$

$$k_3 = [{}^s k_3^{(1,1)} a^1 + {}^s k_3^{(3,1)} a^3 + \mathcal{O}(a^5)]\sin(\phi) + [{}^s k_3^{(3,3)} a^3 + {}^s k_3^{(5,3)} a^5 + \mathcal{O}(a^7)]\sin(3\phi) + \cdots, \tag{42b}$$

$$\mathbf{s}_\perp = [{}^s\mathbf{s}_\perp^{(2,2)} a^2 + {}^s\mathbf{s}_\perp^{(4,2)} a^4 + \mathcal{O}(a^6)]\sin(2\phi) + [{}^s\mathbf{s}_\perp^{(4,4)} a^4 + {}^s\mathbf{s}_\perp^{(6,4)} a^6 + \mathcal{O}(a^8)]\sin(4\phi) + \cdots, \tag{42c}$$

$$s_3 = [{}^c s_3^{(0,0)} a^0 + {}^c s_3^{(2,0)} a^2 + \mathcal{O}(a^4)]\cos(0\phi) + [{}^c s_3^{(2,2)} a^2 + {}^c s_3^{(4,2)} a^4 + \mathcal{O}(a^6)]\cos(2\phi) + \cdots, \tag{42d}$$

$$m = [{}^c m^{(0,0)} a^0 + {}^c m^{(2,0)} a^2 + \mathcal{O}(a^4)]\cos(0\phi) + [{}^c m^{(2,2)} a^2 + {}^c m^{(4,2)} a^4 + \mathcal{O}(a^6)]\cos(2\phi) + \cdots. \tag{42e}$$

Each of these equations makes specific predictions (at leading order in a, at next-to-leading order, and so on) for how the final-state quantities should vary as a function of a and ϕ. We hope that in the future many of these predictions will be tested in detail.

Currently, there are 7 simulations to which we can compare our predictions: the 6 "B-series" simulations in [7], plus one additional ($\phi = 0$) simulation from an earlier work by the same group [11]. We summarize the relevant simulations in Appendix A 3. Although the authors report results for the final kick, as well as the final radiated energy and angular momentum from each simulation, the radiated energy and angular momentum values are not accurate enough to constrain the spin expansion beyond the trivial zeroth-order (constant) term. Therefore, we only consider the final kick. Since the initial spin magnitude is fixed ($a = 0.6$ in all 7 simulations) and only ϕ varies, we should rewrite the expansions (42) in the form (37b). In particular, the expansions for the final kick become

$$\mathbf{k}_\perp = {}^c\mathbf{k}_\perp^{(1)}\cos(\phi) + {}^c\mathbf{k}_\perp^{(3)}\cos(3\phi) + \mathcal{O}(a^5), \tag{43a}$$

$$k_3 = {}^s k_3^{(1)}\sin(\phi) + {}^s k_3^{(3)}\sin(3\phi) + \mathcal{O}(a^5). \tag{43b}$$

As in case 1, only the magnitudes of the final kicks $|\mathbf{k}|$ have been published.[14] Combining Eqs. (43a) and (43b), we find that $|\mathbf{k}|^2 = \mathbf{k}_\perp^2 + k_3^2$ has the expansion

$$|\mathbf{k}|^2 = A_0 + A_2\cos(2\phi) + A_4\cos(4\phi) + \mathcal{O}(a^6), \tag{44}$$

[13] Herrmann *et al.* [7] proposed a general kick formula [their Eq. (5)] inspired by the Kidder formula for the emission of linear momentum [49]. This formula is linear in the initial spins and agrees with ours to this order. A key difference is that they claim their formula is only valid when the initial spin components are determined at *entrance*, when the binary reaches the "last" orbit or plunge. We claim that symmetry and the inclusion of higher-order terms allows our formula to be a valid approximation at *any* initial separation.

[14] Herrmann *et al.* [7] show the individual components of $\mathbf{k}$ in their Fig. 10, but without sufficient numerical precision to allow us to constrain higher-order terms.

TABLE VI. Fits of the kick magnitudes $|\mathbf{k}|^{\rm num}$ listed in Table XV to the fitting formula of Eq. (44). The first column lists the a dependence of the highest-order term appearing in the fit; remaining columns provide the best-fit values for the amplitudes A_i in units of $(\mathrm{km/s})^2$. The first row describes a fit to the two second-order terms in Eq. (44), while the second row provides best-fit values to all three terms that appear to fourth order in a.

Order	A_0	A_2	A_4
Up to a^2	5.04×10^5	-4.23×10^5	$\cdots$
Up to a^4	5.05×10^5	-4.20×10^5	-3.92×10^3

where the amplitudes A_i are given by

$$A_0 \equiv \tfrac{1}{2}[|{}^c\mathbf{k}_\perp^{(1)}|^2 + ({}^sk_3^{(1)})^2], \tag{45a}$$
$$A_2 \equiv \tfrac{1}{2}[|{}^c\mathbf{k}_\perp^{(1)}|^2 - ({}^sk_3^{(1)})^2] + {}^c\mathbf{k}_\perp^{(1)}\cdot{}^c\mathbf{k}_\perp^{(3)} + {}^sk_3^{(1)}{}^sk_3^{(3)}, \tag{45b}$$
$$A_4 \equiv {}^c\mathbf{k}_\perp^{(1)}\cdot{}^c\mathbf{k}_\perp^{(3)} - {}^sk_3^{(1)}{}^sk_3^{(3)}. \tag{45c}$$

Note that the expansion (44) only contains terms of the form $\cos(2n\phi)$, just as we would expect for a quantity with $P=+1$ and $PX=+1$, like m or s_3. However, since $|\mathbf{k}|^2$ is a composite quantity constructed from the more fundamental quantities $\mathbf{k}_\perp$ and k_3, the a^0 term is missing from the coefficient A_0, and instead the leading-order term in A_0 is proportional to a^2. This is a crucial physical difference between the expansion for $|\mathbf{k}|^2$ and the expansions for m and s_3 which both contain a nonvanishing a^0 term.

When we fit the 7 simulations to the second-order and fourth-order forms of Eq. (44), the $\chi^2/\mathrm{d.o.f.}$ is 8.36×10^{-4} and 3.30×10^{-4}, respectively. The corresponding best-fit values for the amplitudes A_i are listed in Table VI, and the second-order fit itself is displayed in Fig. 5.[15] We see that the A_0 and A_2 terms already provide an excellent fit to the simulations of [7], and there is only marginal evidence for the A_4 term. In order to definitively detect the presence of the A_4 term, additional simulations would be needed.

D. Case 4: Herrmann *et al.* "S-series"

In this section we consider the "S-series" simulations of Herrmann *et al.* [7], in which the black holes have equal mass ($q=1$), and spins initially given by

[15]Herrmann *et al.* [7] found that the angle ϕ (their $\hat{\theta}$) remains unchanged during the final few orbits of inspiral, allowing them to apply their kick formula using the *initial* spin components rather than those at entrance. Their quantities $\{V^x_{\rm max}, V^y_{\rm max}, V^z_{\rm max}\}$ correspond directly to our $\{{}^ck_1^1, {}^ck_2^1, {}^sk_3^1\}$, leading to values $A_0 = 5.02\times 10^5\ (\mathrm{km/s})^2$, $A_0 = -4.20\times 10^5\ (\mathrm{km/s})^2$ consistent with our results.

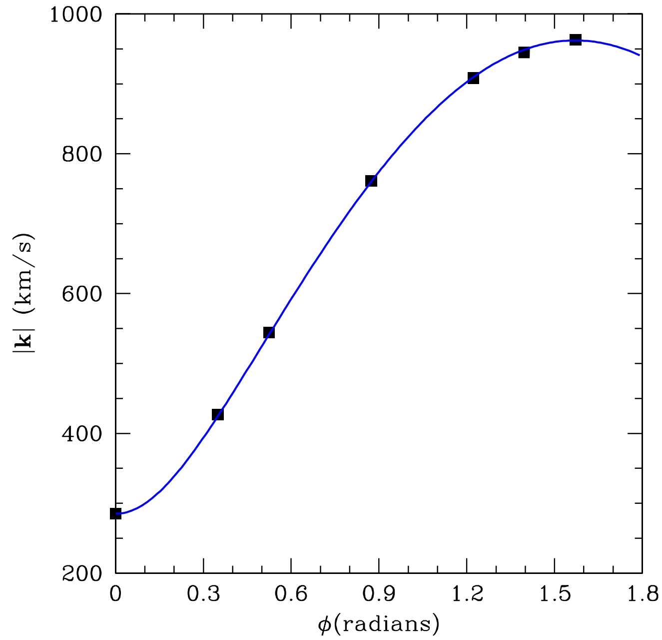

FIG. 5 (color online). The kick magnitudes $|\mathbf{k}|$ as a function of polar angle ϕ for the case 3 configuration given by Eq. (41). The square points correspond to the simulations listed in Table XV, while the blue curve shows the second-order fit to Eq. (44) with amplitudes listed in Table VI.

$$\begin{pmatrix} a_1\\ a_2\\ a_3\end{pmatrix} = \begin{pmatrix} -a\\ 0\\ 0\end{pmatrix}, \qquad \begin{pmatrix} b_1\\ b_2\\ b_3\end{pmatrix} = \begin{pmatrix} a\sin\phi\\ 0\\ a\cos\phi\end{pmatrix}. \tag{46}$$

This is the least symmetric spin configuration that we have considered so far. Since the configuration is parametrized by two numbers (a and ϕ) instead of six (a_i and b_i), we should again use the expansions (37). In particular, since all 22 simulations in this series have the same spin magnitude $a=0.6$, we should write the expansion in the form (37b). Because of the lack of symmetry, most of the expansion coefficients $\{{}^cf^{(j)}, {}^sf^{(j)}\}$ are nonvanishing. In Appendix B 4, we provide relations between these new expansion coefficients and the original spin-expansion coefficients $f^{m_1m_2m_3|n_1n_2n_3}$.

We first consider the final spin $J^z_{\rm final}$ in the $\mathbf{e}^{(3)}$ direction, and the total energy $E_{\rm rad}$ emitted in gravitational radiation during the inspiral. Both of these quantities have expansions of the same form as that of the final mass m, so it is convenient to analyze them in parallel. As indicated by the fits listed in Table VII, there is little evidence for terms beyond linear order in a in either expansion. These linear-order fits are shown in Fig. 6. These same linear terms, of the form $X^{000|001}b_3$, appeared in our analysis of (anti) aligned configurations (case 1). They can be understood physically by the same arguments presented in the final paragraph of that subsection. Though estimates of $E_{\rm rad}$ are not available for case 1, we can attempt a quantitative

TABLE VII. Fits for the z component of the final black hole spin $J^z_{\rm final}/M^2$ and radiated energy $E_{\rm rad}/M$ in case 4. The first column gives the observable being fitted. The second column lists the χ^2/d.o.f. for the best fit. Remaining columns provide the best-fit values for the listed parameters.

Order	0th	1st	2nd	3rd
χ^2/d.o.f.	0.321	3.96×10^{-3}	1.29×10^{-3}	9.95×10^{-4}
${}^c(J^z_{\rm final}/M^2)^0$	0.610	0.617	0.618	0.618
${}^c(J^z_{\rm final}/M^2)^1$	$\cdots$	6.91×10^{-2}	6.84×10^{-2}	6.85×10^{-2}
${}^s(J^z_{\rm final}/M^2)^1$	$\cdots$	$\cdots$	-5.95×10^{-3}	-5.78×10^{-3}
${}^c(J^z_{\rm final}/M^2)^2$	$\cdots$	$\cdots$	-5.15×10^{-3}	-5.26×10^{-3}
${}^s(J^z_{\rm final}/M^2)^2$	$\cdots$	$\cdots$	$\cdots$	7.31×10^{-5}
${}^c(J^z_{\rm final}/M^2)^3$	$\cdots$	$\cdots$	$\cdots$	-2.34×10^{-3}
χ^2/d.o.f.	1.476	0.0508	0.0174	0.0161
${}^c(E_{\rm rad}/M)^0$	3.45×10^{-2}	3.66×10^{-2}	3.68×10^{-2}	3.68×10^{-2}
${}^c(E_{\rm rad}/M)^1$	$\cdots$	8.71×10^{-3}	8.82×10^{-3}	8.82×10^{-3}
${}^s(E_{\rm rad}/M)^1$	$\cdots$	$\cdots$	-1.36×10^{-3}	-1.41×10^{-3}
${}^c(E_{\rm rad}/M)^2$	$\cdots$	$\cdots$	2.57×10^{-4}	3.25×10^{-4}
${}^s(E_{\rm rad}/M)^2$	$\cdots$	$\cdots$	$\cdots$	-1.37×10^{-4}
${}^c(E_{\rm rad}/M)^3$	$\cdots$	$\cdots$	$\cdots$	3.43×10^{-4}

comparison between the final spins $J^z_{\rm final}/M^2$ here and values of s_3 provided for that configuration. Equating these expansions term-by-term at zeroth and first order in a, we find

$$ {}^c(J^z_{\rm final}/M^2)^0 \simeq s_3^{000|000}(m^{000|000})^2, \quad (47a)$$

$$ {}^c(J^z_{\rm final}/M^2)^1 \simeq [s_3^{001|000}(m^{000|000})^2 + 2s_3^{000|000}m^{000|000}m^{001|000}]a. \quad (47b)$$

Inserting the appropriate values from Tables IV and VII into the right- and left-hand sides of Eq. (47), respectively, yields close agreement between ${}^c(J^z_{\rm final}/M^2)^0 = 0.617$ and $s_3^{000|000}(m^{000|000})^2 = 0.626$ and between ${}^c(J^z_{\rm final}/M^2)^1 = 6.91\times10^{-2}$ and $[s_3^{001|000}(m^{000|000})^2 + 2s_3^{000|000}m^{000|000}m^{001|000}]a = 6.96\times10^{-2}$. This agreement is well within the systematic errors

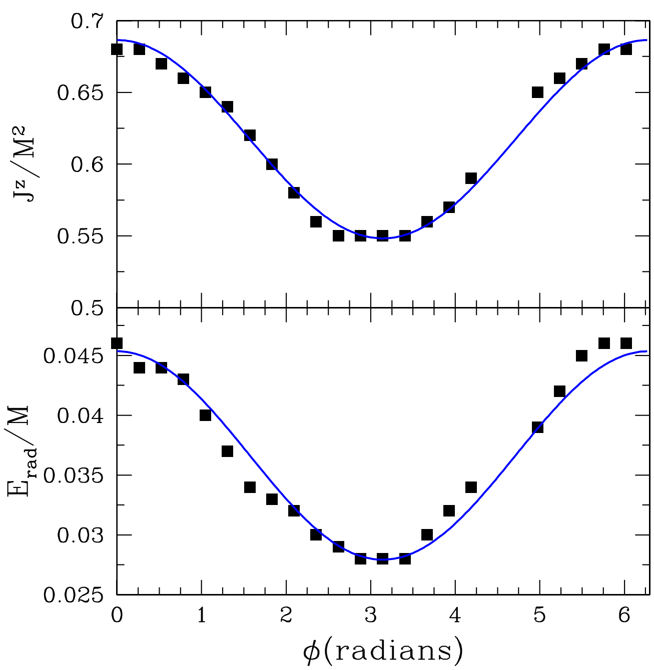

FIG. 6 (color online). The z component of the final spin $J^z_{\rm final}$ and radiated energy $E_{\rm rad}$ as functions of the polar angle ϕ between the spin $\mathbf{b}$ of black hole B and the orbital angular momentum in the configuration of case 4. The square points correspond to the simulations listed in Table XVI, while the blue curves show the linear fit to Eq. (37b) with the first-order coefficients listed in Table VII.

TABLE VIII. Fits of the squared kick magnitudes $|\mathbf{k}|^2$ listed in Table XVI to the fitting formula of Eq. (48). The first column shows the coefficients being fitted, while the second, third, and fourth columns list the numerical values for these coefficients when fits are performed to first, second, and third order, respectively, in a for the individual components of the kicks. The magnitudes of the coefficients are given in units of $({\rm km/s})^2$.

	1st order	2nd order	3rd order
χ^2/d.o.f.	19.5	12.8	1.50
${}^cK^{(0)}$	6.33×10^4	3.19×10^4	4.87×10^5
${}^cK^{(1)}$	$\cdots$	-6.16×10^4	-3.03×10^6
${}^cK^{(2)}$	2.75×10^4	7.08×10^5	2.92×10^6
${}^sK^{(2)}$	$\cdots$	2.81×10^5	2.53×10^6
${}^cK^{(3)}$	$\cdots$	1.99×10^5	9.99×10^6
${}^sK^{(3)}$	$\cdots$	$\cdots$	8.27×10^6
${}^cK^{(4)}$	$\cdots$	-5.36×10^5	-2.95×10^6
${}^sK^{(4)}$	$\cdots$	$\cdots$	-8.70×10^5
${}^cK^{(5)}$	$\cdots$	$\cdots$	-6.53×10^6
${}^cK^{(6)}$	$\cdots$	$\cdots$	-3.05×10^6

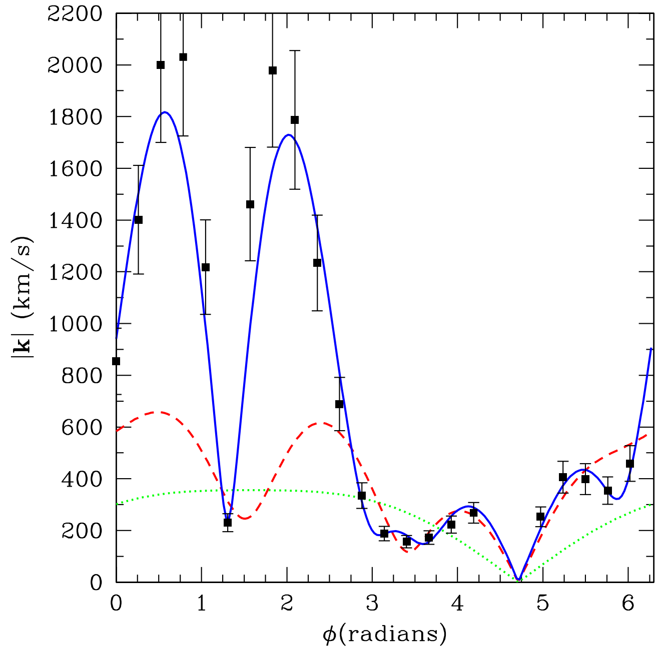

FIG. 7 (color online). The magnitude $|\mathbf{k}|$ of the recoil velocity in km/s as a function of the polar angle ϕ between the spin $\mathbf{b}$ of black hole B and the orbital angular momentum in the configuration of case 4. The square points correspond to the simulations listed in Table XVI, while the green (dotted), red (dashed), and blue (solid) curves show the best fits of Eq. (48c) to these simulations using terms derived from expanding Eqs. (48a) and (48b) to first, second, and, third order in a, respectively. The error bars correspond to 1σ errors of 15% in the kick magnitudes $|\mathbf{k}|$ reported by Herrmann *et al.* [7] as the accuracy of their simulations.

attributed to each series of simulations, and suggests that our approach of decoupling spin-dependent effects term by term shows promise. Further simulations will be necessary to determine how well this promise is fulfilled.

We now turn our attention to the black-hole kicks. As in the case of the "B-series" considered in the previous subsection, our analysis is hampered by only having access to the magnitude of the kicks rather than their individual components. In order to most clearly illuminate the degeneracies that remain between terms in our general expansion (25), we must unfortunately resort to yet another new expansion for this configuration. We expand the individual components and squared magnitude as

$$\mathbf{k}_\perp = \sum_{m=0}^{\infty} \cos^m(\theta)[{}^c\mathbf{k}_\perp^{(m)} + {}^s\mathbf{k}_\perp^{(m)}\sin(\theta)], \tag{48a}$$

$$k_3 = \sum_{m=0}^{\infty} \cos^m(\theta)[{}^ck_3^{(m)} + {}^sk_3^{(m)}\sin(\theta)], \tag{48b}$$

$$|\mathbf{k}|^2 = \sum_{m=0}^{\infty} \cos^m(\theta)[{}^cK^{(m)} + {}^sK^{(m)}\sin(\theta)]. \tag{48c}$$

As previously, we relate the coefficients in this new expansion to those in the general expansion in Appendix B 4. This new expansion is useful because to third order, ${}^ck_3^{(0)} = {}^sk_3^{(0)}$ implying that ${}^cK^{(0)} = {}^sK^{(0)}$ and ${}^cK^{(1)} = {}^sK^{(1)}$. There are therefore only 2 independent terms in the expansion of $|\mathbf{k}|^2$ when $\mathbf{k}_\perp$ and k_3 are expanded to first order in a. The number of independent terms in the expansion of $|\mathbf{k}|^2$ increases to 6 when $\mathbf{k}_\perp$ and k_3 are expanded to second order in a, and increases again to 10 when the components are expanded to third order. The independent coefficients at each order and their best-fit numerical values are listed in Table VIII, while the fits themselves are displayed in Fig. 7. The error bars in this case are proportional to the kick magnitudes $|\mathbf{k}|$ themselves unlike in cases 1 and 2. This implies that our best-fit spin expansions will naturally agree more closely with the smaller values of $|\mathbf{k}|$.

The angular dependence of the numerically determined kicks in this configuration is highly nontrivial, and seems to challenge the linear Kidder kick formulas contemplated previously in the literature [5,7]. These formulas can be reconciled with the numerical results by recognizing that they are linear not in the *initial* spins, but in the spins evaluated at *merger*. Both $\vec{V}_{\rm recoil}$ in Eq. (1) of [5] and $\mathbf{V}$ in Eq. (5) of [7] depend on the angles

$$\Theta_f^{(i)} \equiv \cos^{-1}(\mathbf{\Sigma}\cdot\mathbf{m}^{(i)}) \tag{49}$$

between

$$\mathbf{\Sigma} \equiv M\left(\frac{\mathbf{b}}{M_b} - \frac{\mathbf{a}}{M_a}\right) \tag{50}$$

and the components $\mathbf{m}^{(i)}$ of an orthonormal triad defined at merger. Our triad $\{\mathbf{e}^{(i)}\}$ was defined at the beginning of the simulation. For configurations like case 4 that lack high degrees of symmetry, the initial spins appearing in $\mathbf{\Sigma}$ will precess during the inspiral and the orientation of the triad $\{\mathbf{m}^{(i)}\}$ will vary with respect to a fixed frame. This implies that the angles $\Theta_f^{(i)}$ appearing in the Kidder formulas implicitly depend on the initial spins, introducing nonlinearity into the formulas. We attempt to capture this nonlinear spin dependence explicitly in our spin expansions, allowing us to construct fitting formulas that only depend on genuine *initial* conditions.

The price we pay for making this spin dependence explicit is more complicated nonlinear fitting formulas, as well as a more cumbersome explicit procedure for relating expansions calibrated at different initial stages of the inspiral. This procedure for relating different expansions will be provided in the second paper of this series. An example of how our nonlinear fitting formulas might arise from the linear Kidder formulas can be seen in the configurations of case 4. According to Eq. (5) of [7],

$$k_3 \propto \mathbf{\Sigma} \cdot (K_n \mathbf{m}^{(1)} + K_k \mathbf{m}^{(2)}). \tag{51}$$

Post-Newtonian expansions [49] reveal that to linear order the triad $\{\mathbf{m}^{(i)}(\mathbf{a}, \mathbf{b})\}$ for equal-mass spinning BBHs is related to that in the nonspinning case by

$$\begin{pmatrix} \mathbf{m}^{(1)}(\mathbf{a}, \mathbf{b}) \\ \mathbf{m}^{(2)}(\mathbf{a}, \mathbf{b}) \\ \mathbf{m}^{(3)}(\mathbf{a}, \mathbf{b}) \end{pmatrix} = \begin{pmatrix} \cos\Psi & \sin\Psi & 0 \\ -\sin\Psi & \cos\Psi & 0 \\ 0 & 0 & 1 \end{pmatrix} \begin{pmatrix} \mathbf{m}^{(1)}(0, 0) \\ \mathbf{m}^{(2)}(0, 0) \\ \mathbf{m}^{(3)}(0, 0) \end{pmatrix}, \tag{52}$$

where Ψ is linear in $a_3 + b_3$. If we Taylor expand Ψ in Eq. (52) and then insert both Eqs. (50) and (52) into the Kidder formula (51), terms proportional to $a_1(a_3 + b_3)^n$ emerge. We thus see one way in which a formula linear in the spins at *merger* can become nonlinear in the *initial* spins.

This indeed may be part of the story explaining the numerical results in case 4. The most surprising feature of the "S-series" kicks is the small kick velocity of 230 km/s at $\phi = 75°$. This spin orientation is quite close to the superkick configuration ($\phi = 90°$) at which one would naively expect the kicks to be maximized. While the *amplitude* of the Kidder formula for k_3 is indeed maximized at $\phi = 90°$, Eq. (51) predicts that the superkick should have a sinusoidal dependence on the azimuthal angle at merger as seen in case 2. This angle will depend on the total phase accumulated between the beginning of the simulation and merger. The numerical results for the S-series listed in the final column of Table XVI indicate that the duration of the inspiral varies as $\cos\phi$ (linear in $a_3 + b_3$). The orbital frequency of equal-mass nonspinning BBHs at merger is about $\omega \simeq 0.15 M^{-1}$ [56], suggesting a final orbital period $\tau = 2\pi/\omega \simeq 42M$. This estimate of the period is quite comparable to the difference in merger times $177.3M - 138.6M = 38.7M$ between the successive peaks in $|\mathbf{k}|$ at $\phi = 45°$ and $\phi = 105°$. If this effect is indeed responsible for the observed kicks in case 4, it helps to explain which third-order terms are more significant than in previous cases. Further simulations are necessary to determine if this explanation is correct, and how best to account for it in our formalism.

E. Case 5: Generically oriented initial spins

Finally, we consider the set of 8 equal-mass simulations published in Tichy and Marronetti [10]. Each simulation has a different initial spin configuration, and most of these configurations have no particular symmetry. The initial configurations are *not* chosen according to a pattern, but are instead intended to be "generic." In contrast to previous subsections, there is no natural way to parametrize them in terms of one or two numbers. This means that, again in contrast to previous subsections, we cannot use symmetries and degeneracies to significantly reduce the "effective" number of coefficients in the spin expansion. We must therefore truncate our spin expansions at an order for which the number of independent terms is fewer than the number of simulated data points if we hope to nontrivially test our formalism.

For each of the 8 simulations in [10], the authors quote the final kick *magnitude* $|\mathbf{k}|$, the final spin *magnitude* $|\mathbf{s}|$, and the final mass m. Is this enough information to test the spin-expansion formalism? The answer is "no" for $|\mathbf{k}|$, and "yes" for $|\mathbf{s}|$ and m. In the previous subsections, we have seen that in the general case we should go to second or even third order in the spin expansion to achieve a good fit for $|\mathbf{k}|$; but already at second order, the independent coefficients in the general spin expansion for $|\mathbf{k}|$ outnumber the 8 values of $|\mathbf{k}|$ provided by [10]. Thus, we cannot use the $|\mathbf{k}|$ data to perform a nontrivial test. The situation for m (and even for $|\mathbf{s}|$) is better because, as we have seen in previous subsections, the linear terms in the spin expansion seem sufficient to provide a good fit to the data (except in special symmetric cases where these linear terms vanish, so that the second-order terms become important). Let us test whether this simple behavior continues to hold for the generic initial spin configurations of [10]. At linear order, the mass and spin magnitude are given by

$$m = m^{000|000} + m^{001|000}(a_3 + b_3), \tag{53a}$$

$$\mathbf{s}_\perp = \mathbf{s}_\perp^{100|000}(a_1 + b_1) + \mathbf{s}_\perp^{010|000}(a_2 + b_2), \tag{53b}$$

$$s_3 = s_3^{000|000} + s_3^{001|000}(a_3 + b_3), \tag{53c}$$

$$|\mathbf{s}| = \sqrt{|\mathbf{s}_\perp|^2 + s_3^2}. \tag{53d}$$

The four coefficients $\{m^{000|000}, m^{001|000}, s_3^{000|000}, s_3^{001|000}\}$ were already accurately determined by the large set of simulations in case 1. We therefore fix these coefficients to the values listed in Table IV. Equation (53a) thus predicts the final mass m *with zero free parameters*. If we Taylor

TABLE IX. Fits to the final masses m and spin magnitudes $|\mathbf{s}|$ of the simulations listed in Appendix A 5. The first row lists the χ^2/d.o.f. of fits of Eq. (53a); we use the values of the coefficients determined in case 1 leaving *no* free parameters. The second row shows fits of Eq. (54) to $|\mathbf{s}|$; using the appropriate coefficients determined from case 1 again leaves no free parameters. The third row fits the full formula of Eq. (53d) to $|\mathbf{s}|$; we list the χ^2/d.o.f. and best-fit values of the 3 new parameters.

Quantity	Results
m Eq. (53a)	χ^2/d.o.f. $= 0.275$ 0 free parameters
$\|\mathbf{s}\|$ Eq. (54)	χ^2/d.o.f. $= 0.671$ 0 free parameters
$\|\mathbf{s}\|$ Eq. (53d)	χ^2/d.o.f. $= 0.0707$ 3 free parameters: $\|\mathbf{s}_\perp^{100\|000}\| \approx 0.1871$ $\|\mathbf{s}_\perp^{010\|000}\| \approx 0.2086$ $\cos\Theta \approx -0.974$

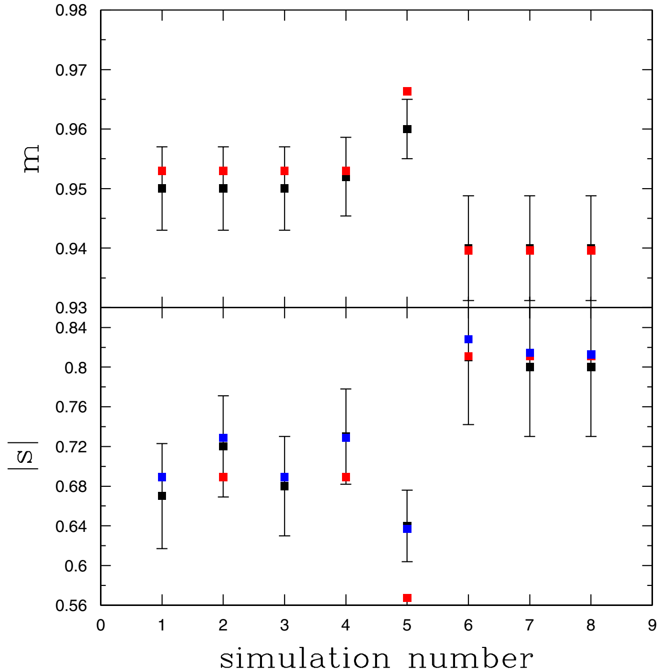

FIG. 8 (color online). Final masses m and spin magnitudes $|\mathbf{s}|$ for the 8 simulations A_i of case 5 listed by simulation number i. The black points show the numerically determined values and 1σ error bars listed in Appendix A 5. The red points in the top and bottom panels show the predictions of Eqs. (53a) and (54), respectively. These use the best-fit values of coefficients obtained in case 1 and fit *no* additional parameters. The blue points in the bottom panel show the best fit of Eq. (53d) to $|\mathbf{s}|$, with coefficients listed in Table IX.

expand the square root in Eq. (53d) for $|\mathbf{s}|$, keeping terms up to linear order in the initial spins, we obtain

$$|\mathbf{s}| \approx s_3^{000|000} + s_3^{001|000}(a_3 + b_3), \tag{54}$$

which again has *no free parameters*. Alternatively, if we do *not* Taylor expand the square root in Eq. (53d), then the expression for $|\mathbf{s}|$ has three free parameters: the magnitudes of the coefficients $\mathbf{s}_\perp^{100|000}$ and $\mathbf{s}_\perp^{010|000}$ and the angle Θ between them. In Table IX, we list the χ^2/d.o.f. and the best-fit values of any free parameters from fitting to Eqs. (53a), (53d), and (54). The fits themselves are shown in Fig. 8.

The goodness of these fits speaks for itself. The most remarkable result is that Eqs. (53a) and (54)—which have no free parameters and only depend on $a_3 + b_3$—do an excellent job (red points in Fig. 8). For all their importance in generating the "superkicks," the components of the initial spins in the orbital plane $\{a_1, a_2, b_1, b_2\}$ seem to have little effect on the final masses and spins. Only one simulation (5) is fit poorly by the red points; not surprisingly it is the configuration with the *largest* spin projection in the orbital plane. The red points *overpredict* m by failing to account for the energy carried away by the gravitational radiation sourced by the planar spins, and *underpredict* $|\mathbf{s}|$ by neglecting the contribution of $\mathbf{s}_\perp$. These results are provocative, but remain provisional until verified by further simulations.

V. CALIBRATING THE SPIN EXPANSION WITH NEW SIMULATIONS

In this section, we suggest a relatively small set of simulations (10 equal-mass simulations, and 16 unequal-mass simulations) with initial spin configurations specially chosen to allow *all* of the spin-expansion coefficients up to second order to be determined uniquely. Once the spin expansion is calibrated in this way, it becomes fully predictive—i.e. it predicts the simulated observables (to second-order accuracy), for *any* initial spin configuration.

This section is organized into four subsections. Subsection V A explains why currently available simulations are *not* sufficient to calibrate the spin expansion. Subsections V B and V C suggest an explicit choice of 10 - equal-mass and 16 unequal-mass simulations with initial spin configurations suitable for this calibration, and provide corresponding formulas for the spin-expansion coefficients in terms of the results of these simulations. Subsection V D collects several additional comments for readers who are interested in pursuing or extending the program suggested here. The *importance* of performing these simulations is discussed later in Sec. VI.

In Appendix D, we generalize the calibration procedure to take account of the inevitable systematic errors arising from the simulations themselves and from truncating the spin expansion at finite order. In particular, given N simulations of known covariance, we derive the minimum-variance unbiased estimators for the spin-expansion coefficients, as well as the corresponding covariance matrix for these estimators.

A. Breaking degeneracies

In the previous section, we examined in detail the predictions of the spin expansion for the 5 different configurations (cases 1–5) that have been simulated to date. Although at first glance it might seem that the total number of currently available simulations is more than sufficient to calibrate all of the expansion coefficients up to second order, in practice we had to perform new fits for each of the 5 configurations. These new fits were required for three distinct reasons. First, many published works have only provided the final kick and spin *magnitudes* $|\mathbf{k}|$ and $|\mathbf{s}|$, not the individual components k_i and s_i. Combining the spin expansions for individual components to predict final magnitudes introduces degeneracies between terms.

Second, many of the available simulation sets study the *same* highly symmetric configurations—like spins aligned with the orbital angular momentum (case 1), or the superkick configuration (case 2). These particular configurations have justifiably garnered much of the attention, both because of their astrophysical interest and because they cleanly illustrate several key features of spinning BBH merger. Nevertheless, since the initial spin components in these configurations are either purely aligned with the orbital angular momentum (case 1) or purely perpendicular (case 2), they fail to constrain the coupling between aligned and perpendicular spin components allowed by symmetry beyond linear order. We found that such terms were required to attain a good fit to the kicks of case 4, suggesting that further simulations are indeed necessary to determine the coefficients of these terms.

Third, different groups performed their simulations at *different* values of the initial dimensionless orbital separation $r/(M_a + M_b)$. Recall, however, from Sec. II that our spin-expansion coefficients are defined at a *fixed* value of $r/(M_a + M_b)$—or, more generally, at a fixed value of the dimensionless inspiral parameter ψ. While post-Newtonian techniques may be able to relate the spin-expansion coefficients at different values of ψ, doing so will add an additional layer of complication and potential systematic error to the calibration process. We treat this issue in a forthcoming paper.

As *existing* simulations are insufficient to fully constrain the spin expansion, in the following subsections we explicitly provide the initial spin configurations for a small number of *new* simulations with which we will be able to achieve the desired calibration. Since our spin-expansion coefficients remain functions of the mass ratio q, a new set of simulations is required in principle at *each* value of q. In practice, we hope that the q dependence of our coefficients is sufficiently smooth that we can interpolate between coefficients calibrated at a small set of mass ratios.

B. Equal-mass ($q = 1$) BBH mergers

Final quantities for equal-mass ($q = 1$) BBH mergers are characterized by their eigenvalues ± 1 under parity P and exchange X. In this subsection, we will use the 4 variables $\{w, x, y, z\}$ to denote generic final quantities with the 4 possible combinations of these eigenvalues as shown in Table X.

To second order in the spin expansion, w, x, y, and z are given by

$$\begin{aligned} w = {} & w^{000|000} + w^{001|000}(a_3 + b_3) + w^{002|000}(a_3^2 + b_3^2) \\ & + w^{200|000}(a_1^2 + b_1^2) + w^{020|000}(a_2^2 + b_2^2) \\ & + w^{110|000}(a_1 a_2 + b_1 b_2) + w^{100|010}(a_1 b_2 + b_1 a_2) \\ & + w^{100|100} a_1 b_1 + w^{010|010} a_2 b_2 + w^{001|001} a_3 b_3, \end{aligned} \tag{55a}$$

$$\begin{aligned} x = {} & x^{001|000}(a_3 - b_3) + x^{002|000}(a_3^2 - b_3^2) \\ & + x^{200|000}(a_1^2 - b_1^2) + x^{020|000}(a_2^2 - b_2^2) \\ & + x^{110|000}(a_1 a_2 - b_1 b_2) + x^{100|010}(a_1 b_2 - b_1 a_2), \end{aligned} \tag{55b}$$

$$\begin{aligned} y = {} & y^{100|000}(a_1 + b_1) + y^{010|000}(a_2 + b_2) \\ & + y^{101|000}(a_1 a_3 + b_1 b_3) + y^{011|000}(a_2 a_3 + b_2 b_3) \\ & + y^{100|001}(a_1 b_3 + b_1 a_3) + y^{010|001}(a_2 b_3 + b_2 a_3), \end{aligned} \tag{55c}$$

$$\begin{aligned} z = {} & z^{100|000}(a_1 - b_1) + z^{010|000}(a_2 - b_2) \\ & + z^{101|000}(a_1 a_3 - b_1 b_3) + z^{011|000}(a_2 a_3 - b_2 b_3) \\ & + z^{100|001}(a_1 b_3 - b_1 a_3) + z^{010|001}(a_2 b_3 - b_2 a_3). \end{aligned} \tag{55d}$$

Note that the expansions for x, y, and z each contain 6 coefficients, while the w expansion has 10 coefficients.

In Table XI, we suggest a set of 10 simulations designed to determine all the coefficients of Eq. (55) at the minimum computational cost. We name these 10 configurations $\{\mathrm{eq0}, \ldots, \mathrm{eq9}\}$. The rth simulation ($r = 0, \ldots, 9$) has initial spin components $\{a_i^{(r)}, b_i^{(r)}\}$, and leads to final-state values $w = w^{(r)}$, $x = x^{(r)}$, $y = y^{(r)}$, and $z = z^{(r)}$.

In each of the proposed simulations, only those initial spin components listed in Table XI are nonzero. Although

TABLE X. Eigenvalues under P and X for the generic final quantities w, x, y, and z, in subsection V B, along with examples of physical quantities with these transformation properties.

	w	x	y	z
P	$+1$	$+1$	-1	-1
X	$+1$	-1	$+1$	-1
E.g.	m, s_3	k_1, k_2	s_1, s_2	k_3

TABLE XI. A suggested set of 10 simulations (denoted eq0–eq9) which can simultaneously determine all of the coefficients up to second order in the general spin expansions, Eqs. (55), for equal-mass ($q = 1$) BBH merger. For each simulation, we list the nonvanishing initial spin components. These spin components may all be chosen independently apart from the requirement that the values of a_3 differ between simulations eq3 and eq4 ($a_3^{(3)} \neq a_3^{(4)}$). While many different sets of configurations satisfy this requirement, it is particularly convenient to choose the set given by Eq. (56).

eq0: none
eq1: a_1
eq2: a_2
eq3: a_1, a_3
eq4: b_1, a_3
eq5: a_1, a_2, a_3
eq6: a_1, b_2, a_3
eq7: a_1, b_1
eq8: a_2, b_2
eq9: a_3, b_3
N.B. $a_3^{(3)} \neq a_3^{(4)}$

all 10 of the simulations $\{eq0, \ldots, eq9\}$ are necessary to determine the w expansion coefficients, only the 6 simulations $\{eq1, \ldots, eq6\}$ are required to determine the x, y, and z coefficients. Thus, if one judges that a 10-simulation set is too expensive for one's computational budget, the 6 simulations $\{eq1, \ldots, eq6\}$ provide a less ambitious but still useful alternative (for example, they fully calibrate the expansion for the kick components k_i).

The simulations in Table XI lift all degeneracies up to second order in the initial spins. *Any* choice for the values of the nonvanishing initial spin components $\{a_i^{(r)}, b_i^{(r)}\}$ in this table will yield a unique solution for all of the coefficients, provided $a_3^{(3)} \neq a_3^{(4)}$. We can use this additional freedom to make the final expressions (57) for the expansion coefficients in terms of the simulated observables $\{w^{(r)}, x^{(r)}, y^{(r)}, z^{(r)}\}$ as algebraically simple as possible. In particular, if we choose the initial nonvanishing spin components in Table XI to satisfy

$$\begin{aligned} \alpha_1 &\equiv +a_1^{(1)} = +a_1^{(3)} = +b_1^{(4)} = +a_1^{(5)} = +a_1^{(6)}, \\ \alpha_2 &\equiv +a_2^{(2)} = +a_2^{(5)} = +b_2^{(6)}, \\ \alpha_3 &\equiv +a_3^{(3)} = -a_3^{(4)} = +a_3^{(5)} = +a_3^{(6)} \end{aligned} \tag{56}$$

then Eqs. (55) can be inverted to yield the simple result

$$\begin{aligned} w^{000|000} &= w^{(0)}, \\ w^{200|000} &= \bar{w}^{(1)}/\alpha_1^2, \\ w^{020|000} &= \bar{w}^{(2)}/\alpha_2^2, \\ w^{110|000} &= [\bar{w}^{(5)} - \bar{w}^{(3)} - \bar{w}^{(2)}]/\alpha_1\alpha_2, \\ w^{100|010} &= [\bar{w}^{(6)} - \bar{w}^{(3)} - \bar{w}^{(2)}]/\alpha_1\alpha_2, \\ w^{002|000} &= [\bar{w}^{(4)} + \bar{w}^{(3)} - 2\bar{w}^{(1)}]/2\alpha_3^2, \\ w^{001|000} &= [\bar{w}^{(3)} - \bar{w}^{(4)}]/2\alpha_3, \\ w^{100|100} &= [\bar{w}^{(7)} - 2\bar{w}^{(1)}]/\alpha_1^2, \\ w^{010|010} &= [\bar{w}^{(8)} - 2\bar{w}^{(2)}]/\alpha_2^2, \\ w^{001|001} &= [\bar{w}^{(9)} - 2\bar{w}^{(3)} + 2\bar{w}^{(1)}]/\alpha_3^2, \end{aligned} \tag{57a}$$

$$\begin{aligned} x^{200|000} &= x^{(1)}/\alpha_1^2, \\ x^{020|000} &= x^{(2)}/\alpha_2^2, \\ x^{110|000} &= [x^{(5)} - x^{(3)} - x^{(2)}]/\alpha_1\alpha_2, \\ x^{100|010} &= [x^{(6)} - x^{(3)} + x^{(2)}]/\alpha_1\alpha_2, \\ x^{002|000} &= [x^{(3)} + x^{(4)}]/2\alpha_3^2, \\ x^{001|001} &= [x^{(3)} - x^{(4)} - 2x^{(1)}]/2\alpha_3, \end{aligned} \tag{57b}$$

$$\begin{aligned} y^{100|000} &= y^{(1)}/\alpha_1, \\ y^{010|000} &= y^{(2)}/\alpha_2, \\ y^{101|000} &= +[y^{(3)} - y^{(1)}]/\alpha_1\alpha_3, \\ y^{100|001} &= -[y^{(4)} - y^{(1)}]/\alpha_1\alpha_3, \\ y^{011|000} &= +[y^{(5)} - y^{(3)} - y^{(2)}]/\alpha_2\alpha_3, \\ y^{010|001} &= +[y^{(6)} - y^{(3)} - y^{(2)}]/\alpha_2\alpha_3, \end{aligned} \tag{57c}$$

$$\begin{aligned} z^{100|000} &= z^{(1)}/\alpha_1, \\ z^{010|000} &= z^{(2)}/\alpha_2, \\ z^{101|000} &= +[z^{(3)} - z^{(1)}]/\alpha_1\alpha_3, \\ z^{100|001} &= +[z^{(4)} + z^{(1)}]/\alpha_1\alpha_3, \\ z^{011|000} &= +[z^{(5)} - z^{(3)} - z^{(2)}]/\alpha_2\alpha_3, \\ z^{010|001} &= -[z^{(6)} - z^{(3)} + z^{(2)}]/\alpha_2\alpha_3, \end{aligned} \tag{57d}$$

where we have defined $\bar{w}^{(r)} \equiv w^{(r)} - w^{000|000}$.

Once Eqs. (55) have been calibrated with the 10 simulations $\{eq0, \ldots, eq9\}$, they can predict the results of *any* additional equal-mass simulations to second-order accuracy.

C. Unequal-mass ($q \neq 1$) BBH mergers

Calibrating the spin-expansion coefficients for unequal-mass ($q \neq 1$) BBH mergers proceeds similarly to the equal-mass case discussed in the previous subsection.

Without loss of generality, we can choose $0 < q < 1$, since exchange symmetry X relates coefficients for mass ratios q and $1/q$. However, at a fixed value of $q(\neq 1)$, exchange X no longer restricts the terms appearing in the expansions. So, for the purposes of this section, there are only two types of final quantities: scalars and pseudoscalars. Scalars (like $\{m, k_1, k_2, s_3\}$) will be represented by the variable u, while pseudoscalars (like $\{s_1, s_2, k_3\}$) will be represented by v.

To second order in the spin expansion, u and v are given by

$$\begin{aligned} u = {}& u^{000|000} + u^{200|000}a_1^2 + u^{000|200}b_1^2 + u^{020|000}a_2^2 + u^{000|020}b_2^2 + u^{001|000}a_3 + u^{000|001}b_3 + u^{002|000}a_3^2 + u^{000|002}b_3^2 \\ &+ u^{110|000}a_1a_2 + u^{000|110}b_1b_2 + u^{100|010}a_1b_2 + u^{010|100}b_1a_2 + u^{100|100}a_1b_1 + u^{010|010}a_2b_2 + u^{001|001}a_3b_3, \end{aligned} \tag{58a}$$

$$\begin{aligned} v = {}& v^{100|000}a_1 + v^{000|100}b_1 + v^{010|000}a_2 + v^{000|010}b_2 + v^{101|000}a_1a_3 + v^{000|101}b_1b_3 + v^{011|000}a_2a_3 + v^{000|011}b_2b_3 \\ &+ v^{100|001}a_1b_3 + v^{001|100}b_1a_3 + v^{010|001}a_2b_3 + v^{001|010}b_2a_3. \end{aligned} \tag{58b}$$

Note that the expansion for u contains 16 coefficients, while the expansion for v contains 12 coefficients.

In Table XII, we suggest a minimal set of 16 simulations needed to simultaneously determine all of the coefficients in Eqs. (58). We have named these configurations $\{\text{uneq0}, \ldots, \text{uneq15}\}$. As in the equal-mass case, the rth simulation ($r = 0, \ldots, 15$) has initial spin components $\{a_i^{(r)}, b_i^{(r)}\}$, and leads to final simulated observables $u = u^{(r)}$ and $v = v^{(r)}$. In each of the proposed simulations, only the initial spin components listed in Table XII are nonzero. While all 16 of the simulations $\{\text{uneq0}, \ldots, \text{uneq15}\}$ are required to determine the u expansion coefficients, the 12 simulations $\{\text{uneq1}, \ldots, \text{uneq12}\}$ suffice to calibrate the v coefficients. If one is only interested in final quantities with odd parity (like s_1, s_2, and k_3), one can reduce the computing time by $\sim 25\%$ by only performing the 12 simulations $\{\text{uneq1}, \ldots, \text{uneq12}\}$.

The simulations in Table XII yield a unique solution for all of the coefficients in Eqs. (58), as long as one chooses $a_3^{(5)} \neq a_3^{(6)}$ and $b_3^{(7)} \neq b_3^{(8)}$. As before, one can choose the values $\{a_i^{(r)}, b_i^{(r)}\}$ appearing in this table to make the inversion of Eqs. (58) particularly simple. If these initial spin components satisfy

$$\begin{aligned}
\alpha_1 &\equiv +a_1^{(1)} = +a_1^{(5)} = +a_1^{(9)} = +a_1^{(11)} = +a_1^{(13)},\\
\alpha_2 &\equiv +a_2^{(2)} = +a_2^{(6)} = +a_2^{(10)} = +a_2^{(12)} = +a_2^{(13)},\\
\alpha_3 &\equiv +a_3^{(5)} = -a_3^{(6)} = +a_3^{(9)} = -a_3^{(10)} = +a_3^{(15)},\\
\beta_1 &\equiv +b_1^{(3)} = +b_1^{(7)} = +b_1^{(9)} = +b_1^{(12)} = +b_1^{(14)},\\
\beta_2 &\equiv +b_2^{(4)} = +b_2^{(8)} = +b_2^{(10)} = +b_2^{(11)} = +b_2^{(14)},\\
\beta_3 &\equiv +b_3^{(7)} = -b_3^{(8)} = -b_3^{(11)} = +b_3^{(12)} = +b_3^{(15)},
\end{aligned} \tag{59}$$

the inverted equations for the spin-expansion coefficients take the comparatively simple form

$$\begin{aligned}
u^{000|000} &= u^{(0)},\\
u^{200|000} &= \bar{u}^{(1)}/\alpha_1^2,\\
u^{020|000} &= \bar{u}^{(2)}/\alpha_2^2,\\
u^{000|200} &= \bar{u}^{(3)}/\beta_1^2,\\
u^{000|020} &= \bar{u}^{(4)}/\beta_2^2,\\
u^{100|100} &= [\bar{u}^{(9)} - \bar{u}^{(5)} - \bar{u}^{(3)}]/\alpha_1\beta_1,\\
u^{010|010} &= [\bar{u}^{(10)} - \bar{u}^{(6)} - \bar{u}^{(4)}]/\alpha_2\beta_2,\\
u^{100|010} &= [\bar{u}^{(11)} - \bar{u}^{(8)} - \bar{u}^{(1)}]/\alpha_1\beta_2,\\
u^{010|100} &= [\bar{u}^{(12)} - \bar{u}^{(7)} - \bar{u}^{(2)}]/\alpha_2\beta_1,\\
u^{110|000} &= [\bar{u}^{(13)} - \bar{u}^{(2)} - \bar{u}^{(1)}]/\alpha_1\alpha_2,\\
u^{000|110} &= [\bar{u}^{(14)} - \bar{u}^{(4)} - \bar{u}^{(3)}]/\beta_1\beta_2,\\
u^{001|000} &= [(\bar{u}^{(5)} - \bar{u}^{(1)}) - (\bar{u}^{(6)} - \bar{u}^{(2)})]/2\alpha_3,\\
u^{002|000} &= [(\bar{u}^{(5)} - \bar{u}^{(1)}) + (\bar{u}^{(6)} - \bar{u}^{(2)})]/2\alpha_3^2,\\
u^{000|001} &= [(\bar{u}^{(7)} - \bar{u}^{(3)}) - (\bar{u}^{(8)} - \bar{u}^{(4)})]/2\beta_3,\\
u^{000|002} &= [(\bar{u}^{(7)} - \bar{u}^{(3)}) + (\bar{u}^{(8)} - \bar{u}^{(4)})]/2\beta_3^2,\\
u^{001|001} &= [\bar{u}^{(15)} - \bar{u}^{(7)} - \bar{u}^{(5)} + \bar{u}^{(3)} + \bar{u}^{(1)}]/\alpha_3\beta_3,
\end{aligned} \tag{60a}$$

$$\begin{aligned}
v^{100|000} &= v^{(1)}/\alpha_1,\\
v^{010|000} &= v^{(2)}/\alpha_2,\\
v^{000|100} &= v^{(3)}/\beta_1,\\
v^{000|010} &= v^{(4)}/\beta_2,\\
v^{101|000} &= +[v^{(5)} - v^{(1)}]/\alpha_1\alpha_3,\\
v^{011|000} &= -[v^{(6)} - v^{(2)}]/\alpha_2\alpha_3,\\
v^{000|101} &= +[v^{(7)} - v^{(3)}]/\beta_1\beta_3,\\
v^{000|011} &= -[v^{(8)} - v^{(4)}]/\beta_2\beta_3,\\
v^{001|100} &= +[v^{(9)} - v^{(5)} - v^{(3)}]/\beta_1\alpha_3,\\
v^{001|010} &= -[v^{(10)} - v^{(6)} - v^{(4)}]/\beta_2\alpha_3,\\
v^{100|001} &= -[v^{(11)} - v^{(8)} - v^{(1)}]/\alpha_1\beta_3,\\
v^{010|001} &= +[v^{(12)} - v^{(7)} - v^{(2)}]/\alpha_2\beta_3,
\end{aligned} \tag{60b}$$

where we have defined $\bar{u}^{(r)} \equiv u^{(r)} - u^{000|000}$.

TABLE XII. A suggested set of 16 unequal-mass ($q \neq 1$) simulations that constitute a minimum set necessary to calibrate the spin-expansion coefficients in Eq. (58). For each simulation, we list the nonvanishing initial spin components. These spin components may all be chosen independently, apart from the constraints $a_3^{(5)} \neq a_3^{(6)}$ and $b_3^{(7)} \neq b_3^{(8)}$, but it is particularly convenient to choose components that satisfy Eq. (59).

uneq0: none
uneq1: a_1
uneq2: a_2
uneq3: b_1
uneq4: b_2
uneq5: a_1, a_3
uneq6: a_2, a_3
uneq7: b_1, b_3
uneq8: b_2, b_3
uneq9: a_1, b_1, a_3
uneq10: a_2, b_2, a_3
uneq11: a_1, b_2, b_3
uneq12: b_1, a_2, b_3
uneq13: a_1, a_2
uneq14: b_1, b_2
uneq15: a_3, b_3
N.B. $a_3^{(5)} \neq a_3^{(6)}$, $b_3^{(7)} \neq b_3^{(8)}$

Once this calibration has been achieved, Eqs. (58) will predict the simulated observables to second-order accuracy, for *any* initial spin configuration.

D. Technical points

In this final subsection, we collect a few additional remarks that will be of interest to readers who wish to pursue or extend the program suggested in this section.

So far, we have discussed the initial spin *orientations* necessary for calibrating the expansion coefficients. What about their absolute *magnitudes* $|\mathbf{a}|$ and $|\mathbf{b}|$? It is best to choose the initial spins to be rather *small* for two reasons. First, the errors introduced by neglecting terms beyond second order are fractionally smaller for small initial spins. The values of the coefficients given by Eqs. (57) and (60) will therefore be closer to their true, unbiased values. The second point relates to the way in which initial conditions for simulations are presently specified. Most groups currently take the 3-metric γ_{ij} on the initial 3-dimensional spatial hypersurface to be conformally flat. While an isolated, nonspinning (Schwarzschild) black hole has conformally flat spatial hypersurfaces, a spinning (Kerr) black hole does not [57] and neither do BBHs (spinning or nonspinning). As the initial spins increase, choosing the initial γ_{ij} to be conformally flat is expected to become an increasingly poor description of realistic BBH initial data. This choice will therefore lead to correspondingly larger systematic errors in determining the coefficients in the spin expansion. The initial spins should be chosen small enough to minimize these problems, yet large enough that the second-order effects we are seeking are not swamped by other systematic errors in the numerical simulations.

As these systematic errors are inevitable, it may be fruitful to reinterpret the coefficients on the left-hand sides of Eqs. (57) and (60). Instead of regarding these coefficients as the algebraic solutions to Eqs. (55) and (58), we consider them to be *estimators* ($\hat{w}^{m_1 m_2 m_3|n_1 n_2 n_3}, \hat{x}^{m_1 m_2 m_3|n_1 n_2 n_3}, \ldots$) constructed from the simulated observables $\{w^{(r)}, x^{(r)}, \ldots\}$ and the estimated initial spin components $\{a_i^{(r)}, b_i^{(r)}\}$. Once errors are taken into account, it may be desirable to use larger sets of simulations to beat down the noise associated with our estimators. We pursue this approach in Appendix D, where we derive minimum-variance estimators constructed from N simulations, and provide the covariance matrix for these estimators in terms of the covariance matrices associated with the estimated observables $\{w^{(r)}, x^{(r)}, \ldots\}$ and initial spin components $\{a_i^{(r)}, b_i^{(r)}\}$.

In the future, it may be interesting to extend this section's second-order calibration up to third order. Although all of the third-order contributions to the mass m and spin $\mathbf{s}$ identified in Sec. IV were small corrections, the final kicks $\mathbf{k}$ in case 4 seemed to exhibit considerable third-order effects. Recoils for generic initial spin orientations have not yet been adequately simulated to determine whether these third-order effects reflect genuine physical behavior or are merely artifacts of systematic errors within the numerical codes. If spin expansions calibrated to second order according to the program outlined in this section fail to describe BBH mergers with generic initial spin orientations, we may want to test whether a third-order expansion can remedy observed discrepancies. Calibrating to third order will require 12 additional simulations (for a total of $10 + 12 = 22$) in the equal-mass ($q = 1$) case, and 28 additional simulations (for a total of $16 + 28 = 44$) in the unequal-mass ($q \neq 1$) case. In Appendix C we have provided explicit third-order expansions of the 4 variables $\{w, x, y, z\}$ in the equal-mass case. These expansions can be inverted to obtain formulas for the third-order coefficients similar to the second-order inversions of Eqs. (55). These formulas can then be used to identify an optimal choice of 22 simulations from which *all* coefficients up to third order can be calibrated.

VI. DISCUSSION

In this paper, we have developed and tested the "spin-expansion" formalism. This is the following simple idea. Long after merger, we regard any final (dimensionless) quantity f—such as the kick velocity $\mathbf{k}$ or spin vector $\mathbf{s}$ of the final Kerr black hole—as a function $f(\psi, q, a_i, b_i)$ of the 8 "initial" (dimensionless) quantities $\{\psi, q, a_i, b_i\}$ necessary to specify the initial configuration of a BBH in circular orbit. Then we Taylor expand this function around $a_i = b_i = 0$, and use three symmetries (rotation R, parity P, and exchange X) to significantly restrict the terms that can appear in the expansion. Finally, we interpret the leading-order terms in the Taylor expansion as leading-order predictions for f, while the next-to-leading terms in the expansion are the next-to-leading predictions, and so on.

To us, it seems genuinely surprising that the final state of the complicated nonlinear process of binary black hole merger can be usefully described by such a simple-minded approach. This simplicity should be regarded as another discovery which has come from the recent breakthroughs in numerical relativity.

In the introduction to this paper, we listed some of the advantages—both practical and conceptual—of the spin-expansion formalism. It may be helpful to look back at this list, now that we have had a chance to introduce and explore the formalism in detail. Here we would just like to highlight three *new* discoveries which came from applying the spin expansion to simulations in Sec. IV, and which illustrate the potential of this approach.

A. Three highlights

First, we have discovered a new third-order spin dependence of the kick velocities in the superkick configuration considered in Sec. IV B. These third-order modulations, clearly revealed in Fig. 4, are present in the simulations of [5,6] but went unnoticed because with amplitudes less than 100 km/s they are dwarfed by the primary linear superkicks. We were able to find them because the spin expansion made a specific prediction for the next-to-leading contribution: it told us to look for a contribution to k_3 proportional to a^3 with triple the fundamental (linear) superkick frequency. Empirical fitting formulas—linear in spins, and inspired by post-Newtonian results—provide acceptable fits for these superkick simulations, but our discovery shows that there is more to learn if one is willing to go beyond these fitting formulas.

Second, we have discovered a new second-order spin dependence of the radiation energy $E_{\rm rad}$, the radiated angular momentum $J_{\rm rad}$ and the final spin s_3 in the superkick configuration. The spin expansion predicts that, since these three quantities $\{E_{\rm rad}, J_{\rm rad}, s_3\}$ are all characterized by the same transformation properties ($P = +1$, $X = +1$), they should all exhibit the same next-to-leading-order behavior: $A + B\cos(2\phi + \text{phase})$. Again this behavior is present in the simulations of [5,6], and is clearly displayed in Fig. 3; but without the guidance of the spin expansion, it went unnoticed in [5], and was dismissed as a possible numerical artifact in [6].

Third, we wish to highlight the remarkable agreement between the predictions of the spin expansion and the simulations of generically oriented spin configurations [10] considered in Sec. IV E (case 5). This agreement is illustrated in Fig. 8, where the black points are the simulations results and the red points are the predictions. We emphasize that the red points are genuine predictions—i.e. there were *no free parameters* in these fits, since all of the relevant coefficients had already been calibrated by the simulations in case 1. The red and black points only disagree for one of the eight simulations in case 5 and, as explained in Sec. IV E, this disagreement is easily understood. So far, numerical relativists have focused mostly on highly symmetric configurations like the aligned case in Sec. IV A and the superkick configuration of Sec. IV B. This is probably because of the expected complications from nonlinear spin precession in the generic case. Herrmann *et al.* [7] observe these precessions in their "S-series," and note that they make it impossible to use the post-Newtonian-inspired fitting formula for the final kicks in this case. Figure 8 seems to provide evidence that our spin expansions continue to apply, even in the presence of these precession effects.

B. Future directions

Let us end by briefly mentioning a few directions for further study.

First, it would be extremely fruitful to calibrate the spin-expansion coefficients, up to second or third order. As explained in Sec. V, currently available simulations leave many degeneracies among spin-expansion coefficients, even at first and second order. To rectify this problem, in Sec. V we suggest a small set of simulations—10 equal-mass simulations and 16 unequal-mass simulations—and explicitly show how these would uniquely determine all of the spin-expansion coefficients up to second order. Once these coefficients are calibrated in this way, the spin expansion becomes fully predictive: given *any* initial spin configuration, it predicts the final results $\{m, k_i, s_i\}$ with second-order accuracy. In addition to facilitating tests of the spin expansion, it is clear that this result—a set of simple formulas which predict the final state of BBH merger given the initial state—would be of enormous interest from the standpoint of astrophysical and cosmological applications. For example, our spin expansion precisely encapsulates the relevant information for incorporating the recent discoveries of numerical relativity into cosmological simulations of BBH merger in the context of structure formation. It would also be interesting from a purely theoretical standpoint. The initial spin configurations we have identified in Sec. V provide a systematic approach for seeking qualitatively *new* behavior in the unexplored regions of BBH parameter space. Any unexpected constraints, patterns, or relationships among the calibrated coefficients (beyond the ones we have used thus far in our construction) could indicate interesting new dynamical effects or symmetries of the system.

Second, we have mentioned that a final quantity f may be regarded as function on an 8-dimensional space $\{\psi, q, a_i, b_i\}$. The spin expansion elucidates the structure of the 6-dimensional subspace parametrized by $\{a_i, b_i\}$, but we would also like to know the behavior along the ψ and q directions. In a follow-up paper, we consider how post-Newtonian techniques may be used to to explore the ψ dependence of the spin-expansion coefficients. Some insights may be gained by an analogy with effective field theory, where the renormalized coupling constants depend on the momentum scale at which they are defined, although the physical predictions of the theory do not. Determining the q dependence of the spin-expansion coefficients [23] seems less straightforward, and is an interesting topic for future research.

ACKNOWLEDGMENTS

We thank Antony Lewis and Jonathan Sievers for access to a modified version of COSMOMC [62], a FORTRAN 90 Markov-chain Monte-Carlo engine that was used to double-check the fits in this paper. We would also like to thank Emanuele Berti, Alessandra Buonanno, Neal Dalal, Peter Diener, Nils Dorband, Larry Kidder, Luis Lehner, Carlos Lousto, Pedro Marronetti, Samaya Nissanke, Harald Pfeiffer, Eric Poisson, Denis Pollney, Christian Reisswig, Luciano Rezzolla, Eric Schnetter, Bela Szilagyi, Wolfgang Tichy, Bill Unruh, Daniel Wesley, and Yosef Zlochower for useful discussions.

TABLE XIII. Final mass data for case 1: equal-mass ($q = 1$) binary black holes with spins aligned (or antialigned) with the orbital angular momentum. Points A_1– A_4 are from [11], points B_1– B_9 are from [13], and points C_1– C_{11} are from [16].

	a_3	b_3	$m^{\rm num}$
A_1	0.2	−0.2	0.9526 ± 0.0023
A_2	0.4	−0.4	0.9521 ± 0.0017
A_3	0.6	−0.6	0.9519 ± 0.0014
A_4	0.8	−0.8	0.9521 ± 0.0028
B_1	0.584	−0.584	0.9536 ± 0.0049
B_2	0.584	−0.438	0.9507 ± 0.0049
B_3	0.584	−0.292	0.9482 ± 0.0049
B_4	0.584	−0.146	0.9461 ± 0.0049
B_5	0.584	0	0.9439 ± 0.0049
B_6	0.584	0.146	0.9412 ± 0.0049
B_7	0.584	0.292	0.9376 ± 0.0049
B_8	0.584	0.438	0.9344 ± 0.0049
B_9	0.584	0.584	0.9315 ± 0.0049
C_1	−0.90	−0.90	0.970 ± 0.004
C_2	−0.75	−0.75	0.968 ± 0.004
C_3	−0.50	−0.50	0.963 ± 0.004
C_4	−0.25	−0.25	0.958 ± 0.004
C_5	0.0	0.0	0.951 ± 0.004
C_6	0.25	0.25	0.944 ± 0.004
C_7	0.50	0.50	0.933 ± 0.004
C_8	0.62	0.62	0.926 ± 0.004
C_9	0.75	0.75	0.916 ± 0.004
C_{10}	0.82	0.82	0.909 ± 0.004
C_{11}	0.90	0.90	0.906 ± 0.004

APPENDIX A: TABLES OF SIMULATED FINAL KICKS, SPINS, AND MASSES

1. Case 1: $q = 1$, $\mathbf{a}_\perp = \mathbf{b}_\perp = 0$

We use the 28 simulations of [14] with nonzero recoils to test our expansions for the final kicks in the case of equal-mass ($q = 1$) binary black holes with spins aligned (or antialigned) with the orbital angular momentum. This is the largest and most recent series of simulations for this configuration published at the time this manuscript was prepared. The numerical estimates of $|\mathbf{k}_\perp|$ are available in Table 1 of [14]. We adopt their 1σ errors of 8 km/s for the kick magnitude.

We constrain our expansion for the final spin s_3 by performing a joint fit to the full set of 38 simulations in [14] and the 10 simulations of [16] that they consider to be relatively free from the numerical dissipation of angular momentum. We use the proposed 1σ errors of 0.01 and 0.02 for the simulations of [14,16], respectively.

To constrain our expansion for the final mass m, we perform a joint fit to 3 series of simulations [11,13,16], as each series consists of only a small number of individual simulations. These simulations are summarized in Table XIII. For points A_1– A_4 we assume fractional errors on the radiated energy identical to those provided in [11] for the final kicks. For points B_1– B_9 we assume errors on the final masses of 0.5% of the initial energy $M_{\rm ADM}$, as [13] only claims to conserve energy to this accuracy. Finally, we

TABLE XIV. Data for case 2: equal-mass ($q = 1$) binary black holes with equal and opposite spins in the orbital plane. Points A_1–A_6 are from [5], while points B_1–B_{12} are from [6]. These papers present final quantities different from those discussed in this paper, but whose spin dependence can be readily analyzed in our formalism. The scalar $J_{\rm rad}$ is the total angular momentum radiated in gravitational waves, listed in units of M^2 where $M \equiv M_a + M_b$ is the sum of the horizon masses of the initial binary black holes. $\%E_{\rm rad}$ is the percentage of the initial energy radiated in gravitational waves.

	a	ϕ	$k_3^{\rm num}$	$J_{\rm rad}/M^2$	$\%E_{\rm rad}$
A_1	0.515	1.571	1833 ± 30	0.248 ± 0.003	3.63 ± 0.01
A_2	0.515	0.785	1093 ± 10	0.244 ± 0.003	3.53 ± 0.01
A_3	0.515	3.142	352 ± 10	0.246 ± 0.004	3.57 ± 0.01
A_4	0.515	4.712	−1834 ± 30	0.249 ± 0.003	3.63 ± 0.01
A_5	0.515	3.304	47 ± 10	0.245 ± 0.005	3.55 ± 0.02
A_6	0.515	0.0	−351 ± 10	0.246 ± 0.003	3.57 ± 0.02
	a	ϕ	$k_3^{\rm num}$	s_3	...
B_1	0.723	0.0	2680 ± 94	0.6859 ± 0.0009	
B_2	0.723	0.524	2310 ± 94	0.6856 ± 0.0009	
B_3	0.723	1.047	1150 ± 94	0.6897 ± 0.0009	
B_4	0.723	1.571	−340 ± 94	0.6931 ± 0.0009	
B_5	0.723	2.094	−1590 ± 94	0.6934 ± 0.0009	
B_6	0.723	2.618	−2400 ± 94	0.6892 ± 0.0009	
B_7	0.723	3.142	−2690 ± 94	0.6859 ± 0.0009	
B_8	0.723	3.665	−2320 ± 94	0.6856 ± 0.0009	
B_9	0.723	4.189	−1160 ± 94	0.6897 ± 0.0009	
B_{10}	0.723	4.712	320 ± 94	0.6932 ± 0.0009	
B_{11}	0.723	5.236	1580 ± 94	0.6935 ± 0.0009	
B_{12}	0.723	5.760	2400 ± 94	0.6892 ± 0.0009	

TABLE XV. Data for case 3: equal-mass $(q = 1)$ binary black holes with equal and opposite spins in the $\mathbf{e}^{(1)} - \mathbf{e}^{(3)}$ plane. Point A is from [11] while points B_1–B_6 are from [7]. $J_{\rm rad}/L_0^z$ is the ratio of the total radiated angular momentum to the initial orbital angular momentum, while $E_{\rm rad}/M$ is the ratio of the total radiated energy to the sum of the initial horizon masses. We do not include estimates of the radiated energy and angular momentum for point A because this simulation began at a different initial separation and orbital angular momentum from points B_1–B_6. Herrmann *et al.* [7] claimed 15% errors on their reported numbers which we treat here as true 1σ bars.

	a	ϕ	$\lvert\mathbf{k}\rvert^{\rm num}$	$J_{\rm rad}/L_0^z$	$E_{\rm rad}/M$
A	0.6	0.0	285 ± 12	$\cdots$	$\cdots$
B_1	0.6	0.349	427 ± 64	0.24 ± 0.036	0.033 ± 0.005
B_2	0.6	0.524	544 ± 82	0.24 ± 0.036	0.033 ± 0.005
B_3	0.6	0.873	761 ± 114	0.25 ± 0.038	0.034 ± 0.005
B_4	0.6	1.222	908 ± 136	0.25 ± 0.038	0.034 ± 0.005
B_5	0.6	1.396	945 ± 142	0.25 ± 0.038	0.034 ± 0.005
B_6	0.6	1.571	963 ± 144	0.25 ± 0.038	0.034 ± 0.005

use the highest-resolution simulations of all 11 initial data sets listed in Table I of [16]. While they claim that numerical dissipation of angular momentum makes estimates of s_3 unreliable for $a_3, b_3 > 0.75$, the final masses are largely unaffected as shown in their Fig. 4. We therefore use both simulations with $a_3, b_3 > 0.75$, and assume for all simulations errors on m of 0.004 consistent with their claimed resolution limits.

2. Case 2: $q = 1$, $\mathbf{a}_\perp = -\mathbf{b}_\perp$, $a_3 = b_3 = 0$

The data points for this case are summarized in Table XIV. Campanelli *et al.* [5] provide error estimates for their final observables, which we assume represent true 1σ statistical error bars. Brügmann *et al.* do not provide error estimates for the individual simulated data points B_i; however, they do claim 95% confidence limits of $\pm 2\%$ on their maximum kick amplitude of 2725 km/s and $\pm 5 \times 10^{-4}$ on their mean spin $a_0 = 0.6891$ as determined from the black-hole ringdown. We assume these values correspond to 2σ error bars on each parameters, and that they

TABLE XVI. Data for case 4: equal-mass $(q = 1)$ BBHs belonging to the "S-series" of [7]. The spins have magnitudes $a = 0.6$ and orientations $\mathbf{a} = (-a, 0, 0)$ and $\mathbf{b} = (a \sin\phi, 0, a \cos\phi)$. $J^z_{\rm final}/M^2$ is the z component of the final black hole's spin in units of the sum M of the initial horizon masses, and $E_{\rm rad}/M$ is total radiated energy in units of M. Herrmann *et al.* [7] claimed 15% errors on their reported numbers which we treat here as true 1σ bars. $T_{\rm max}$, measured in units of M, is an estimate of the merger time defined as the coordinate time between the beginning of the simulation and when the Newman-Penrose quantity Ψ_4 is maximized.

	ϕ	$\lvert\mathbf{k}\rvert^{\rm num}$	$J^z_{\rm final}/M^2$	$E_{\rm rad}/M$	$T_{\rm max}$
A_1	0°	854 ± 128	0.68 ± 0.102	0.046 ± 0.0069	192.3
A_2	15°	1401 ± 210	0.68 ± 0.102	0.044 ± 0.0066	189.5
A_3	30°	2000 ± 300	0.67 ± 0.101	0.044 ± 0.0066	184.1
A_4	45°	2030 ± 305	0.66 ± 0.099	0.043 ± 0.0065	177.3
A_5	60°	1218 ± 183	0.65 ± 0.098	0.040 ± 0.0060	168.6
A_6	75°	230 ± 35	0.64 ± 0.096	0.037 ± 0.0056	159.1
A_7	90°	1462 ± 219	0.62 ± 0.093	0.034 ± 0.0051	148.6
A_8	105°	1979 ± 297	0.60 ± 0.090	0.033 ± 0.0050	138.6
A_9	120°	1787 ± 268	0.58 ± 0.087	0.032 ± 0.0048	130.5
A_{10}	135°	1234 ± 185	0.56 ± 0.084	0.030 ± 0.0045	124.1
A_{11}	150°	689 ± 103	0.55 ± 0.083	0.029 ± 0.0044	119.5
A_{12}	165°	335 ± 50	0.55 ± 0.083	0.028 ± 0.0042	117.7
A_{13}	180°	188 ± 28	0.55 ± 0.083	0.028 ± 0.0042	117.7
A_{14}	195°	157 ± 24	0.55 ± 0.083	0.028 ± 0.0042	120.5
A_{15}	210°	173 ± 26	0.56 ± 0.084	0.030 ± 0.0045	125.5
A_{16}	225°	223 ± 33	0.57 ± 0.086	0.032 ± 0.0048	132.7
A_{17}	240°	268 ± 40	0.59 ± 0.089	0.034 ± 0.0051	141.4
A_{18}	285°	253 ± 38	0.65 ± 0.098	0.039 ± 0.0059	174.1
A_{19}	300°	406 ± 61	0.66 ± 0.099	0.042 ± 0.0063	181.8
A_{20}	315°	399 ± 60	0.67 ± 0.101	0.045 ± 0.0068	187.7
A_{21}	330°	354 ± 53	0.68 ± 0.102	0.046 ± 0.0069	191.8
A_{22}	345°	459 ± 69	0.68 ± 0.102	0.046 ± 0.0069	193.2

TABLE XVII. Data for case 5: equal-mass ($q = 1$) BBHs with generic spin orientations taken from [10]. The initial spins have magnitudes $a = 0.8$ and orientations given by traditional spherical coordinates, $\mathbf{a} = (a\sin\theta_a\cos\phi_a, a\sin\theta_a\sin\phi_a, a\cos\theta_a)$ and $\mathbf{b} = (a\sin\theta_b\cos\phi_b, a\sin\theta_b\sin\phi_b, a\cos\theta_b)$.

	θ_a	ϕ_a	θ_b	ϕ_b	M_f/M	J_f/M^2
A_1	90°	180°	90°	0°	0.95 ± 0.0070	0.67 ± 0.053
A_2	90°	225°	90°	315°	0.95 ± 0.0070	0.72 ± 0.051
A_3	45°	90°	135°	270°	0.95 ± 0.0070	0.68 ± 0.050
A_4	45°	270°	135°	270°	0.952 ± 0.0066	0.73 ± 0.048
A_5	60°	90°	60°	90°	0.96 ± 0.0050	0.64 ± 0.036
A_6	90°	270°	0°	0°	0.94 ± 0.0088	0.81 ± 0.068
A_7	90°	240°	0°	0°	0.94 ± 0.0088	0.80 ± 0.070
A_8	90°	210°	0°	0°	0.94 ± 0.0088	0.80 ± 0.070

were derived from 12 independent data points. This leads to crude 1σ errors of $1/2 \times \sqrt{12} \times 0.02 \times 2725$ km/s $=$ 94 km/s on each kick and $1/2 \times \sqrt{12} \times 0.0005 = 0.0009$ on each final spin.

3. Case 3: Herrmann *et al.* "B-series"

The data for this case are summarized in Table XV.

4. Case 4: Herrmann *et al.* "S-series"

The data for this case are summarized in Table XVI.

5. Case 5: The generic case (Tichy-Marronetti)

The data for this case are summarized in Table XVII. Even at second order in the initial spin magnitude a, there are too many independent nondegenerate coefficients to fit with only 8 simulations. We therefore only attempt to fit the final masses M_f/M and spin magnitudes J_f/M^2 as these can be fit with linear-order terms in our formalism. We assume errors on these quantities that are 20% of the radiated energy $(M_\infty^{\rm ADM} - M_f)/M$ and radiated angular momentum $(J_\infty^{\rm ADM} - J_f)/M^2$.

APPENDIX B: SUPPLEMENTARY EQUATIONS

1. Relations between coefficients for case 1

Here are the relations between the new coefficients A, B, and C, and the original expansion coefficients $\mathbf{k}_\perp^{m_1m_2m_3|n_1n_2n_3}$:

$$A = \frac{|\mathbf{k}_\perp^{002|000}|}{|\mathbf{k}_\perp^{001|000}|}\cos\Theta, \tag{B1a}$$

$$B = \frac{\mathbf{k}_\perp^{001|000}\cdot\mathbf{k}_\perp^{003|000}}{|\mathbf{k}_\perp^{001|000}|^2} + \frac{1}{2}\left(\frac{|\mathbf{k}_\perp^{002|000}|}{|\mathbf{k}_\perp^{001|000}|}\right)^2\sin^2\Theta, \tag{B1b}$$

$$C = \frac{\mathbf{k}_\perp^{001|000}\cdot(\mathbf{k}_\perp^{002|001} - \mathbf{k}_\perp^{003|000})}{|\mathbf{k}_\perp^{001|000}|^2} + 2B, \tag{B1c}$$

where Θ is the angle between $\mathbf{k}_\perp^{001|000}$ and $\mathbf{k}_\perp^{002|000}$.

2. Relations between coefficients for case 2

Here are the relations between the "old" coefficients $f^{m_1m_2m_3|n_1n_2n_3}$ and the new coefficients $f^{(i,j)}$ of subsection IV B:

$$\begin{aligned}
{}^cf^{(0,0)} &= f^{000|000},\\
{}^cf^{(2,0)} &= f^{200|000} + f^{020|000} - \tfrac{1}{2}f^{100|100} - \tfrac{1}{2}f^{010|010},\\
{}^cf^{(2,2)} &= f^{200|000} - f^{020|000} - \tfrac{1}{2}f^{100|100} + \tfrac{1}{2}f^{010|010},\\
{}^sf^{(2,2)} &= f^{110|000} - f^{100|010},
\end{aligned} \tag{B2a}$$

$$\begin{aligned}
{}^cf^{(1,1)} &= 2f^{100|000},\\
{}^sf^{(1,1)} &= 2f^{010|000},\\
{}^cf^{(3,1)} &= \tfrac{3}{2}f^{300|000} - \tfrac{3}{2}f^{200|100} + \tfrac{1}{2}f^{120|000}\\
&\quad - \tfrac{1}{2}f^{020|100} - \tfrac{1}{2}f^{110|010},\\
{}^sf^{(3,1)} &= \tfrac{1}{2}f^{210|000} - \tfrac{1}{2}f^{110|100} - \tfrac{1}{2}f^{200|010}\\
&\quad + \tfrac{3}{2}f^{030|000} - \tfrac{3}{2}f^{020|010},\\
{}^cf^{(3,3)} &= \tfrac{1}{2}f^{300|000} - \tfrac{1}{2}f^{200|100} - \tfrac{1}{2}f^{120|000}\\
&\quad + \tfrac{1}{2}f^{020|100} + \tfrac{1}{2}f^{110|010},\\
{}^sf^{(3,3)} &= \tfrac{1}{2}f^{210|000} - \tfrac{1}{2}f^{110|100} - \tfrac{1}{2}f^{200|010}\\
&\quad - \tfrac{1}{2}f^{030|000} + \tfrac{1}{2}f^{020|010}.
\end{aligned} \tag{B2b}$$

3. Relations between coefficients for case 3

Here are the relations between the old coefficients $f^{m_1m_2m_3|n_1n_2n_3}$ and the new coefficients $f^{(i,j)}$ of subsection IV C. Cosine terms with *even* i, j appear in the expansion of scalars *even* under PX, the observables m and s_3.

$$\begin{aligned}
{}^cf^{(0,0)} &= f^{000|000},\\
{}^cf^{(2,0)} &= f^{002|000} + f^{200|000} - \tfrac{1}{2}f^{001|001} - \tfrac{1}{2}f^{100|100},\\
{}^cf^{(2,2)} &= f^{002|000} - f^{200|000} - \tfrac{1}{2}f^{001|001} + \tfrac{1}{2}f^{100|100}.
\end{aligned} \tag{B3}$$

Cosine terms with *odd* i, j appear in the expansion of $\mathbf{k}_\perp$ because it is a scalar *odd* under PX.

$$\begin{aligned}
{}^c f^{(1,1)} &= 2f^{001|000},\\
{}^c f^{(3,1)} &= \tfrac{3}{2}f^{003|000} - \tfrac{3}{2}f^{002|001} + \tfrac{1}{2}f^{201|000} - \tfrac{1}{2}f^{101|100}\\
&\quad - \tfrac{1}{2}f^{200|001},\\
{}^c f^{(3,3)} &= \tfrac{1}{2}f^{003|000} - \tfrac{1}{2}f^{002|001} - \tfrac{1}{2}f^{201|000} + \tfrac{1}{2}f^{101|100}\\
&\quad + \tfrac{1}{2}f^{200|001}.
\end{aligned} \tag{B4}$$

Sine terms with *odd* i, j appear in the expansion of k_3 because it is a pseudoscalar *odd* under PX.

$$\begin{aligned}
{}^s f^{(1,1)} &= 2f^{100|000},\\
{}^s f^{(3,1)} &= \tfrac{1}{2}f^{102|000} - \tfrac{1}{2}f^{101|001} + \tfrac{1}{2}f^{100|002} + \tfrac{3}{2}f^{300|000}\\
&\quad - \tfrac{3}{2}f^{200|100},\\
{}^s f^{(3,3)} &= \tfrac{1}{2}f^{102|000} - \tfrac{1}{2}f^{101|001} + \tfrac{1}{2}f^{100|002} - \tfrac{1}{2}f^{300|000}\\
&\quad + \tfrac{1}{2}f^{200|100}.
\end{aligned} \tag{B5}$$

Sine terms with *even* i, j appear in the expansion of $\mathbf{s}_\perp$ because it is a pseudoscalar *even* under PX.

$${}^s f^{(2,2)} = f^{101|000} - f^{100|001}. \tag{B6}$$

4. Relations between coefficients for case 4

Here are the relations between the old coefficients $f^{m_1m_2m_3|n_1n_2n_3}$ and the new coefficients $f^{(i,j)}$ of subsection IV D. Coefficients in the expansions of $J^z_{\rm final}/M^2$ and $E_{\rm rad}/M$ behave like those for m, which are provided here.

$$\begin{aligned}
&{}^c m^{(0,0)} = m^{000|000}, \quad {}^c m^{(1,0)} = 0, \quad {}^c m^{(1,1)} = m^{001|000},\\
&{}^s m^{(1,1)} = 0, \quad {}^c m^{(2,0)} = \tfrac{1}{2}(m^{002|000} + 3m^{200|000}),\\
&{}^c m^{(2,1)} = 0, \quad {}^s m^{(2,1)} = -m^{100|100},\\
&{}^c m^{(2,2)} = \tfrac{1}{2}(m^{002|000} - m^{200|000}), \quad {}^s m^{(2,2)} = 0,\\
&{}^c m^{(3,0)} = 0, \quad {}^c m^{(3,1)} = m^{200|001} + \tfrac{1}{4}(3m^{003|000} + m^{201|000}),\\
&{}^s m^{(3,1)} = 0, \quad {}^c m^{(3,2)} = 0, \quad {}^s m^{(3,2)} = -\tfrac{1}{2}m^{101|100},\\
&{}^c m^{(3,3)} = \tfrac{1}{4}(m^{003|000} - m^{201|000}), \quad {}^s m^{(3,3)} = 0.
\end{aligned} \tag{B7}$$

We next provide expressions for the coefficients in the expansions of $\mathbf{k}_\perp$, k_3, and $|\mathbf{k}|^2$ in Eq. (48) in terms of the original coefficients of our general expansion (25).

$${}^c\mathbf{k}_\perp^{(1)} = -\mathbf{k}_\perp^{001|000}a + (\mathbf{k}_\perp^{200|001} - \mathbf{k}_\perp^{201|000})a^3, \tag{B8a}$$
$${}^s\mathbf{k}_\perp^{(1)} = \mathbf{k}_\perp^{101|100}a^3, \tag{B8b}$$
$${}^c\mathbf{k}_\perp^{(2)} = (\mathbf{k}_\perp^{200|000} - \mathbf{k}_\perp^{002|000})a^2, \tag{B8c}$$
$${}^c\mathbf{k}_\perp^{(3)} = (\mathbf{k}_\perp^{201|000} - \mathbf{k}_\perp^{003|000})a^3, \tag{B8d}$$

$${}^c k_3^{(0)} = -k_3^{100|000}a + (k_3^{200|100} - k_3^{300|000})a^3, \tag{B9a}$$
$${}^s k_3^{(0)} = -k_3^{100|000}a + (k_3^{200|100} - k_3^{300|000})a^3, \tag{B9b}$$
$${}^c k_3^{(1)} = -k_3^{100|001}a^2, \tag{B9c}$$
$${}^s k_3^{(1)} = -k_3^{101|000}a^2, \tag{B9d}$$
$${}^c k_3^{(2)} = -(k_3^{200|100} + k_3^{100|002})a^3, \tag{B9e}$$
$${}^s k_3^{(2)} = +(k_3^{300|000} - k_3^{102|000})a^3, \tag{B9f}$$

$${}^c K^{(0)} = {}^c k_3^{(0)2} + {}^s k_3^{(0)2}, \tag{B10a}$$
$${}^s K^{(0)} = 2{}^c k_3^{(0)}{}^s k_3^{(0)}, \tag{B10b}$$
$${}^c K^{(1)} = 2[{}^c k_3^{(0)}{}^c k_3^{(1)} + {}^s k_3^{(0)}{}^s k_3^{(1)}], \tag{B10c}$$
$${}^s K^{(1)} = 2[{}^c k_3^{(0)}{}^s k_3^{(1)} + {}^s k_3^{(0)}{}^s k_3^{(1)}] \tag{B10d}$$
$$\begin{aligned}{}^c K^{(2)} &= |{}^c\mathbf{k}_\perp^{(1)}|^2 + |{}^s\mathbf{k}_\perp^{(1)}|^2 + {}^c k_3^{(1)2} + {}^s k_3^{(1)2}\\ &\quad - {}^s k_3^{(0)2} + 2[{}^c k_3^{(0)}{}^c k_3^{(2)} + {}^s k_3^{(0)}{}^s k_3^{(2)}],\end{aligned} \tag{B10e}$$
$$\begin{aligned}{}^s K^{(2)} &= 2[{}^s\mathbf{k}_\perp^{(1)}\cdot{}^c\mathbf{k}_\perp^{(1)} + {}^c k_3^{(0)}{}^s k_3^{(2)} + {}^s k_3^{(0)}{}^c k_3^{(2)}\\ &\quad + {}^c k_3^{(1)}{}^s k_3^{(1)}],\end{aligned} \tag{B10f}$$
$$\begin{aligned}{}^c K^{(3)} &= 2[{}^c\mathbf{k}_\perp^{(1)}\cdot{}^c\mathbf{k}_\perp^{(2)} + {}^c k_3^{(1)}{}^c k_3^{(2)} + {}^s k_3^{(1)}{}^s k_3^{(2)}\\ &\quad - {}^s k_3^{(0)}{}^s k_3^{(1)}],\end{aligned} \tag{B10g}$$
$${}^s K^{(3)} = 2[{}^s\mathbf{k}_\perp^{(1)}\cdot{}^c\mathbf{k}_\perp^{(2)} + {}^c k_3^{(1)}{}^s k_3^{(2)} + {}^s k_3^{(1)}{}^c k_3^{(2)}], \tag{B10h}$$
$$\begin{aligned}{}^c K^{(4)} &= |{}^c\mathbf{k}_\perp^{(2)}|^2 - |{}^s\mathbf{k}_\perp^{(1)}|^2 + 2{}^c\mathbf{k}_\perp^{(1)}\cdot{}^c\mathbf{k}_\perp^{(3)} + {}^c k_3^{(2)2}\\ &\quad + {}^s k_3^{(2)2} - {}^s k_3^{(1)2} - 2{}^s k_3^{(0)}{}^s k_3^{(2)},\end{aligned} \tag{B10i}$$
$${}^s K^{(4)} = 2[{}^s\mathbf{k}_\perp^{(1)}\cdot{}^c\mathbf{k}_\perp^{(3)} + {}^c k_3^{(2)}{}^s k_3^{(2)}], \tag{B10j}$$
$${}^c K^{(5)} = 2[{}^c\mathbf{k}_\perp^{(2)}\cdot{}^c\mathbf{k}_\perp^{(3)} - {}^s k_3^{(1)}{}^s k_3^{(2)}], \tag{B10k}$$
$${}^c K^{(6)} = |{}^c\mathbf{k}_\perp^{(3)}|^2 - {}^s k_3^{(2)2}. \tag{B10l}$$

APPENDIX C: THIRD-ORDER SPIN EXPANSIONS

In Sec. V B, we identified 10 equal-mass initial spin configurations which when simulated could be used to calibrate all the coefficients appearing in spin expansions of the 4 variables $\{w, x, y, z\}$ up to second order. Here we provide the corresponding third-order terms appearing in those same spin expansions. If desired, these formulas can be used to identify 12 additional equal-mass spin configurations with which these third-order terms may be calibrated. The third-order terms in the expansion for w ($P = +1$, $X = +1$) are

$$\begin{aligned} w = \cdots &+ w^{201|000}(a_1^2a_3 + b_1^2b_3) + w^{021|000}(a_2^2a_3 + b_2^2b_3) + w^{200|001}(a_1^2b_3 + b_1^2a_3) + w^{020|001}(a_2^2b_3 + b_2^2a_3) \\ &+ w^{111|000}(a_1a_2a_3 + b_1b_2b_3) + w^{110|001}(a_1a_2b_3 + b_1b_2a_3) + w^{101|010}(a_1b_2a_3 + b_1a_2b_3) \\ &+ w^{100|011}(a_1b_2b_3 + b_1a_2a_3) + w^{101|100}a_1b_1(a_3 + b_3) + w^{011|010}a_2b_2(a_3 + b_3) + w^{002|001}a_3b_3(a_3 + b_3) \\ &+ w^{003|000}(a_3^3 + b_3^3). \end{aligned} \tag{C1a}$$

The corresponding third-order terms in the expansion for x ($P = +1$, $X = -1$) may be obtained from the above equation for w by making the substitution $w^{m_1m_2m_3|n_1n_2n_3} \rightarrow x^{m_1m_2m_3|n_1n_2n_3}$, and changing " $+$" to " $-$" when it appears in parentheses: $(\cdots + \cdots) \rightarrow (\cdots - \cdots)$.

The third-order terms in the expansion for y ($P = -1$, $X = +1$) are

$$\begin{aligned} y = \cdots &+ y^{200|100}a_1b_1(a_1 + b_1) + y^{020|010}a_1b_1(a_2 + b_2) + y^{110|100}a_2b_2(a_1 + b_1) + y^{110|010}a_2b_2(a_2 + b_2) \\ &+ y^{101|001}a_3b_3(a_1 + b_1) + y^{011|001}a_3b_3(a_2 + b_2) + y^{120|000}(a_1a_2^2 + b_1b_2^2) + y^{210|000}(a_2a_1^2 + b_2b_1^2) \\ &+ y^{020|100}(b_1a_2^2 + a_1b_2^2) + y^{200|010}(b_2a_1^2 + a_2b_1^2) + y^{102|000}(a_1a_3^2 + b_1b_3^2) + y^{012|000}(a_2a_3^2 + b_2b_3^2) \\ &+ y^{100|002}(a_1b_3^2 + b_1a_3^2) + y^{010|002}(a_2b_3^2 + b_2a_3^2) + y^{300|000}(a_1^3 + b_1^3) + y^{030|000}(a_2^3 + b_2^3). \end{aligned} \tag{C1b}$$

The third-order terms in the expansion for z ($P = -1$, $X = -1$) again may be obtained from the above equation for y by making the substitution $y^{m_1m_2m_3|n_1n_2n_3} \rightarrow z^{m_1m_2m_3|n_1n_2n_3}$ and changing " $+$" to " $-$" when it appears inside parentheses: $(\cdots + \cdots) \rightarrow (\cdots - \cdots)$.

APPENDIX D: MINIMUM-VARIANCE ESTIMATORS FOR THE SPIN COEFFICIENTS

In Sec. V we showed how a small number of simulations (10 in the equal-mass case, 16 for unequal masses) can be used to uniquely determine the 10 or 16 coefficients appearing to second order in the spin expansion. In the absence of systematic errors these are all the simulations that would be required, but further simulations may be useful once these errors are taken into account. In this appendix, we will explicitly construct minimum-variance unbiased estimators for the coefficients in the spin expansion from N noisy simulations of known covariance.

We proceed in two steps. In step one, we solve the problem under the assumption that the uncertainties in the initial spins are negligible compared to those in the final quantities. In step two, we explore how our approach might be modified to include the effects of these initial spin uncertainties.

1. Neglecting initial spin uncertainties

Imagine a generic final quantity $f \in \{w, x, y, z, u, v\}$ such as those described in Sec. V. In the ith simulation, with initial spin configuration $\{a_1^{(i)}, a_2^{(i)}, a_3^{(i)}, b_1^{(i)}, b_2^{(i)}, b_3^{(i)}\}$, this quantity will have an estimated value $\hat{f}_i$ that when averaged over different assumptions for the systematic errors is equal to its true value f_i:

$$\langle \hat{f}_i \rangle = f_i. \tag{D1}$$

The systematic errors introduce uncertainty in the values of f estimated for each simulation, and this uncertainty can be described by the covariance matrix for f,

$$F_{ij} \equiv \langle \hat{f}_i\hat{f}_j \rangle - \langle \hat{f}_i \rangle\langle \hat{f}_j \rangle. \tag{D2}$$

Consider N initial spin configurations, which correspond to the N true final values f_i ($i = 1, \ldots, N$). If we truncate the spin expansion at finite order, then, as seen in Eqs. (55) and (58), these N values f_i are a linear combination of D spin-expansion coefficients c_j. Thus we can write the relationship in matrix form as

$$\mathbf{f} = \mathbf{A}\mathbf{c}, \tag{D3}$$

where $\mathbf{f}$ is a column vector with N elements f_i, $\mathbf{c}$ is a column vector with D elements c_j, and $\mathbf{A}$ is an $N \times D$ matrix whose N rows consist of the D combinations of initial spin components in each simulation multiplying the coefficients c_j. For example, when we rewrite Eq. (55b) in the form of Eq. (D3), we have $\mathbf{f} = \{x_1, \ldots, x_N\}$ and $\mathbf{c} = \{x^{001|000}, x^{002|000}, \ldots, x^{100|010}\}$, with $D = 6$. The elements of the matrix A are then easily read off from Eq. (55b), e.g. $A_{41} = (a_3^{(4)} - b_3^{(4)})$.

At least D simulations are required to determine the D coefficients c_j. If this minimum number of simulations $N = D$ are performed and the spin configurations of these simulations are chosen such that the $D \times D$ matrix $\mathbf{A}$ is invertible, then there is a unique estimator

$$\hat{\mathbf{c}} = \mathbf{A}^{-1}\hat{\mathbf{f}} \tag{D4}$$

such that

$$\langle \hat{\mathbf{c}} \rangle = \mathbf{A}^{-1}\langle \hat{\mathbf{f}} \rangle = \mathbf{A}^{-1}\mathbf{A}\mathbf{c} = \mathbf{c}. \tag{D5}$$

Here we have assumed that the initial spin components are known exactly and all the uncertainty lies in the estimated final quantities $\hat{\mathbf{f}}$. We will relax this assumption later in this appendix. The covariance matrix C_{ij} for this estimator is

$$C_{ij} = \langle \hat{c}_i \hat{c}_j \rangle - \langle \hat{c}_i \rangle \langle \hat{c}_j \rangle$$
$$= A_{ik}^{-1} A_{jl}^{-1} \langle \hat{f}_k \hat{f}_l \rangle - A_{ik}^{-1} A_{jl}^{-1} \langle \hat{f}_k \rangle \langle \hat{f}_l \rangle = A_{ik}^{-1} A_{jl}^{-1} F_{kl}, \tag{D6}$$

where here and throughout this appendix we adopt the Einstein convention of summing over repeated indices. In the absence of systematic errors ($F_{ij} = 0$), D simulations would suffice to determine the spin coefficients with perfect accuracy ($C_{ij} = 0$).

With systematic errors present ($F_{ij} \neq 0$), a larger set of simulations ($N > D$) can be used to construct estimators $\hat{\mathbf{c}}$ with lower variance provided these additional simulations are at least partially *uncorrelated*. As the estimated final quantities $\hat{\mathbf{f}}$ are linear in the spin coefficients, our estimator generalizes to

$$\hat{\mathbf{c}} = \mathbf{W} \hat{\mathbf{f}}, \tag{D7}$$

where $\mathbf{W}$ is now a $D \times N$ matrix of linear weights. For this estimator to be unbiased

$$\langle \hat{\mathbf{c}} \rangle = \mathbf{W} \langle \hat{\mathbf{f}} \rangle = \mathbf{W} \mathbf{A} \mathbf{c} = \mathbf{c} \tag{D8}$$

implying that $\mathbf{W}$ must satisfy the constraint

$$\mathbf{W} \mathbf{A} = \mathbf{I}, \tag{D9}$$

where $\mathbf{I}$ is the $D \times D$ identity matrix. The set of N spin configurations to be simulated must be chosen such that $\mathbf{A}$ has a left inverse. Equation (D9) consists of D^2 constraints on the DN elements of $\mathbf{W}$, leaving additional freedom for $N > D$ to choose $\mathbf{W}$ to minimize the covariance

$$C_{ij} = \langle \hat{c}_i \hat{c}_j \rangle - \langle \hat{c}_i \rangle \langle \hat{c}_j \rangle \ = W_{ik} W_{jl} \langle \hat{f}_k \hat{f}_l \rangle - W_{ik} W_{jl} \langle \hat{f}_k \rangle \langle \hat{f}_l \rangle$$

or in matrix notation

$$\mathbf{C} = \mathbf{W} \mathbf{F} \mathbf{W}^T. \tag{D11}$$

As $\mathbf{C}$ is a real, symmetric matrix, it can be decomposed into a real, diagonal eigenvalue matrix $\boldsymbol{\sigma}$ and an orthogonal eigenvector matrix $\mathbf{O}$

$$\mathbf{C} = \mathbf{O} \boldsymbol{\sigma} \mathbf{O}^T. \tag{D12}$$

The columns of $\mathbf{O}$ give the uncorrelated linear combinations of estimators $\hat{c}_i$, while the elements of $\boldsymbol{\sigma}$ give the variances of these combinations. We specifically seek the weight matrix $\mathbf{W}$ that minimizes the sum of these eigenvalues

$$\mathrm{Tr}\, \boldsymbol{\sigma} = \mathrm{Tr} \mathbf{C}. \tag{D13}$$

We can determine this $\mathbf{W}$ by the method of Lagrange multipliers, with a Lagrangian given by

$$L = \mathrm{Tr}[\mathbf{C} + \boldsymbol{\lambda}^T (\mathbf{W} \mathbf{A} - \mathbf{I})], \tag{D14}$$

where $\boldsymbol{\lambda}$ is a $D \times D$ matrix of Lagrange multipliers. Setting the partial derivatives $\partial L / \partial \lambda_{ij}$ to zero yields the $D \times D$ constraint equation (D9), while $\partial L / \partial W_{ij} = 0$ provides the additional $D \times N$ matrix equation

$$2 \mathbf{W} \mathbf{F} + \boldsymbol{\lambda} \mathbf{A}^T = 0. \tag{D15}$$

Equations (D9) and (D15) thus provide $D(N + D)$ linear equations for the D^2 elements of $\boldsymbol{\lambda}$ and DN elements of $\mathbf{W}$. Solving these equations, we find

$$\mathbf{W} = (\mathbf{A}^T \mathbf{F}^{-1} \mathbf{A})^{-1} \mathbf{A}^T \mathbf{F}^{-1}. \tag{D16}$$

To summarize the analysis so far: If we can neglect the errors in the initial spin components $\{a_i^{(r)}, b_i^{(r)}\}$ that go into the construction of $\mathbf{A}$, then the minimum-variance unbiased estimators $\hat{c}_i$ for the spin-expansion coefficients c_i are given by Eq. (D7), with weight matrix $\mathbf{W}$ given by Eq. (D16). These optimal estimators $\hat{c}_i$ will have covariance matrix given by

$$\mathbf{C} = (\mathbf{A}^T \mathbf{F}^{-1} \mathbf{A})^{-1}. \tag{D17}$$

2. Including initial spin uncertainties

Now let us consider the effect of errors in the initial spin components $\{a_i^{(r)}, b_i^{(r)}\}$. One source of these errors is that numerical relativists do not know how to specify the proper initial data corresponding to physical binaries of arbitrary spin. This problem is usually addressed by waiting for the nonphysical "junk radiation" to exit the system, after which the binary is presumed to settle down into a *physical* spin configuration. This physical spin configuration will generally be slightly different than the one relativists had intended to specify, introducing error into the initial spin components $\{a_i^{(r)}, b_i^{(r)}\}$. Techniques exist to measure BBH spins in simulations [17,58–61], so one could measure the initial spins *after* the junk radiation had exited the system, and use these components rather than those supposedly specified by the numerical initial data. However, while at large binary separations the initial spin components of the two black holes are well defined, at finite separations the components are gauge-dependent and different techniques for measuring them yield different results.

To formally address the systematic errors in $\mathbf{A}$ we promote it to an estimator $\hat{\mathbf{A}}$ that on average will provide the correct values

$$\langle \hat{A}_{ij} \rangle = A_{ij} \tag{D18}$$

but will now have a nonzero covariance

$$S_{ijkl} \equiv \langle \hat{A}_{ij} \hat{A}_{kl} \rangle - \langle \hat{A}_{ij} \rangle \langle \hat{A}_{kl} \rangle. \tag{D19}$$

Deriving the truly optimal weight matrix $\mathbf{W}$ that simultaneously minimizes contributions to the covariance from errors in both the final quantities $\hat{\mathbf{f}}$ and initial spins $\hat{\mathbf{A}}$ will be challenging. Since $\mathbf{W}$ is constructed from $\mathbf{A}$ as seen in Eq. (D16), it is itself now an estimator $\hat{\mathbf{W}}$ with its own covariance matrix

$$T_{ijkl} \equiv \langle \hat{W}_{ij}\hat{W}_{kl}\rangle - \langle \hat{W}_{ij}\rangle\langle \hat{W}_{kl}\rangle. \tag{D20}$$

The covariance matrix of our estimator $\hat{\mathbf{c}}$ will now be given by

$$C_{ij} = \langle \hat{c}_i\hat{c}_j\rangle - \langle \hat{c}_i\rangle\langle \hat{c}_j\rangle = \langle \hat{W}_{ik}\hat{W}_{jl}\hat{f}_k\hat{f}_l\rangle - c_ic_j. \tag{D21}$$

To make further progress, we make the possibly invalid assumption that errors in our estimators $\hat{\mathbf{W}}$ and $\hat{\mathbf{f}}$ are *uncorrelated*

$$\langle \hat{W}_{ik}\hat{W}_{jl}\hat{f}_k\hat{f}_l\rangle = \langle \hat{W}_{ik}\hat{W}_{jl}\rangle\langle \hat{f}_k\hat{f}_l\rangle. \tag{D22}$$

This allows us to reduce Eq. (D21) to

$$C_{ij} = W_{ik}W_{jl}F_{kl} + T_{ikjl}f_kf_l + T_{ikjl}F_{kl}. \tag{D23}$$

The first term in Eq. (D23) is the familiar error of Eq. (D10), while the second and third terms proportional to T_{ijkl} reflect the increased covariance due to errors in the initial spins. One might next hope to insert this $\mathbf{C}$ into the Lagrangian L of Eq. (D14) and obtain a new $N \times D$ matrix equation $\partial L/\partial A_{ij} = 0$ to constrain $\mathbf{A}$. Two problems immediately come to mind with this approach. First, once $\mathbf{A}$ has been promoted to an estimator Eqs. (D9) and (D15) become nonlinear in $\mathbf{W}$, $\mathbf{A}$, and $\boldsymbol{\lambda}$ and hence much more difficult to solve. Second, only $6N$ of the DN elements of $\mathbf{A}$ may be chosen independently as there are only 6 initial spin components in each of the N simulations. Possibly this could be addressed by adding new terms to the Lagrangian with new Lagrange multipliers, although this might be difficult to implement.

Leaving the determination of a truly optimal estimator for future work, we choose to stick with the estimator $\hat{\mathbf{c}}$ defined by the weight matrix $\mathbf{W}$ of Eq. (D16). This estimator should remain nearly optimal provided the initial spin errors are subdominant to the other errors coming from the simulations themselves and from truncating the spin expansion at finite order. Now we can account for the errors in the initial spins $\{a_i^{(r)}, b_i^{(r)}\}$ as follows. If these errors have a known probability distribution (e.g. if they are assumed to be Gaussian, with known covariance matrix), then we can generate many Monte Carlo realizations of $\{a_i^{(r)}, b_i^{(r)}\}$, and use these to compute many realizations of $\mathbf{A}$. Next, by inserting these $\mathbf{A}$ realizations into Eqs. (D7) and (D16), we obtain many realizations of $\hat{\mathbf{c}}$. The mean of these $\mathbf{c}$ realizations is our best guess for $\mathbf{c}$, while the covariance of these realizations gives an estimate of the "extra" uncertainty in the estimator $\hat{\mathbf{c}}$ due to the initial spin uncertainties. We can add this extra covariance to the right-hand side of Eq. (D17) to estimate the *total* covariance C_{ij}.

As an alternative to Monte Carlo techniques, we can make further analytic progress by assuming that the errors $\boldsymbol{\delta}\mathbf{A}$ in $\hat{\mathbf{A}}$ are small, in which case the errors $\boldsymbol{\delta}\mathbf{W}$ in $\hat{\mathbf{W}}$ can be linearized in $\boldsymbol{\delta}\mathbf{A}$. Defining

$$\mathbf{N} \equiv \mathbf{A}^T\mathbf{F}^{-1}\mathbf{A}, \tag{D24}$$

we linearize Eq. (D16) to obtain

$$\begin{aligned}\boldsymbol{\delta}\mathbf{W} = \mathbf{N}^{-1}(&\boldsymbol{\delta}\mathbf{A}^T - \boldsymbol{\delta}\mathbf{A}^T\mathbf{F}^{-1}\mathbf{A}\mathbf{N}^{-1}\mathbf{A}^T \\ &- \mathbf{A}^T\mathbf{F}^{-1}\boldsymbol{\delta}\mathbf{A}\mathbf{N}^{-1}\mathbf{A}^T)\mathbf{F}^{-1}.\end{aligned} \tag{D25}$$

This equation allows us to propagate errors and express the covariance T_{ijkl} of $\hat{\mathbf{W}}$ in terms of the covariance S_{ijkl} of $\hat{\mathbf{A}}$. Defining

$$\mathbf{M} \equiv \mathbf{F}^{-1}\mathbf{A}\mathbf{N}^{-1}\mathbf{A}^T \tag{D26}$$

we obtain

$$\begin{aligned}T_{ijkl} &= \langle \delta W_{ij}\delta W_{kl}\rangle \\ &= N_{ia}^{-1}N_{kb}^{-1}F_{jc}^{-1}F_{ld}^{-1}[S_{cadb} + S_{eafb}\mathbf{M}_{ec}\mathbf{M}_{fd} \\ &\quad + S_{efgh}(\mathbf{F}^{-1}\mathbf{A})_{ea}(\mathbf{A}\mathbf{N}^{-1})_{cf}(\mathbf{F}^{-1}\mathbf{A})_{gb}(\mathbf{A}\mathbf{N}^{-1})_{dh} \\ &\quad - 2S_{caef}(\mathbf{F}^{-1}\mathbf{A})_{eb}(\mathbf{A}\mathbf{N}^{-1})_{df} - 2S_{caeb}\mathbf{M}_{ed} \\ &\quad + 2S_{eafg}\mathbf{M}_{ec}(\mathbf{F}^{-1}\mathbf{A})_{fb}(\mathbf{A}\mathbf{N}^{-1})_{dg}].\end{aligned} \tag{D27}$$

Inserting Eq. (D27) in (D23) provides an approximate analytic expression for the extra covariance of the estimator $\hat{\mathbf{c}}$ caused by uncertainties in the initial spins.

APPENDIX E: GENERALIZATION TO NONCIRCULAR (ECCENTRIC) ORBITS

We focused on circular orbits in the body of this paper as gravitational radiation is expected to circularize orbits of most astrophysical systems long before the final stage of the merger [44]. However, our approach readily generalizes to initially noncircular orbits so we felt that a few brief remarks on this subject might be appropriate here. Recall from Sec. II that in the circular case, the initial conditions are specified by 8 dimensionless parameters: the mass ratio q and the dimensionless spins $\{\mathbf{a}, \mathbf{b}\}$ at some initial instant labeled by ψ. We can extend our spin expansion to noncircular orbits by specifying the difference in linear momentum $\mathbf{p} \equiv \mathbf{p}_A - \mathbf{p}_B$ between the two BBHs. As $\mathbf{p}$ lies in the orbital plane, our initial conditions are now specified by $8 + 2 = 10$ numbers.

Apart from this modification, the analysis proceeds just as in Sec. II. We define the same orthonormal triad $\{\mathbf{e}^{(1)}, \mathbf{e}^{(2)}, \mathbf{e}^{(3)}\}$, and consider the maps from the initial quantities to the final quantities

$$f = f(\psi, p_i, q, a_i, b_i). \tag{E1}$$

As in Sec. II, we can constrain these maps through symmetry considerations. Under parity P or exchange X, we have $\mathbf{p} \to -\mathbf{p}$ and $\{\mathbf{e}^{(1)}, \mathbf{e}^{(2)}\} \to -\{\mathbf{e}^{(1)}, \mathbf{e}^{(2)}\}$. Thus, the components p_1 and p_2 are invariant under both P and X. The maps therefore satisfy

$$f(\psi, p_i, q, a_i, b_i) = (\pm)_P f(\psi, p_i, q, \tilde{a}_i, \tilde{b}_i) \tag{E2a}$$

and

$$f(\psi, p_i, q, a_i, b_i) = (\pm)_{PX} f(\psi, p_i, 1/q, b_i, a_i). \quad \text{(E2b)}$$

Since the components p_1 and p_2 have eigenvalues of $+1$ under P and X, the series expansions introduced in Sec. II D still hold, but now the coefficients $f^{m_1 m_2 m_3|n_1 n_2 n_3}$ are functions of ψ, q, *and* p_i. It is probably useful to Taylor expand these coefficients around the point $p_i = p_{i,\mathrm{circ}}$, where $p_{i,\mathrm{circ}}$ is the linear momentum for a circular *non-spinning* orbit at orbital "separation" ψ. In the Newtonian limit, the three parameters $\{\psi, p_1, p_2\}$ specify the semimajor axis, eccentricity, and longitude of pericenter associated with elliptical orbits, respectively. As the BBHs inspiral, they will trace a trajectory through this 3-dimensional parameter space. Using this to relate coefficients defined at different points in the parameter space will be pursued in future work.

[1] F. Pretorius, Phys. Rev. Lett. **95**, 121101 (2005).
[2] J. G. Baker, J. Centrella, D. I. Choi, M. Koppitz, and J. van Meter, Phys. Rev. Lett. **96**, 111102 (2006).
[3] M. Campanelli, C. O. Lousto, P. Marronetti, and Y. Zlochower, Phys. Rev. Lett. **96**, 111101 (2006).
[4] J. A. Gonzalez, M. D. Hannam, U. Sperhake, B. Brügmann, and S. Husa, Phys. Rev. Lett. **98**, 231101 (2007).
[5] M. Campanelli, C. O. Lousto, Y. Zlochower, and D. Merritt, Phys. Rev. Lett. **98**, 231102 (2007).
[6] B. Brügmann, J. A. Gonzalez, M. Hannam, S. Husa, and U. Sperhake, arXiv:0707.0135 [Phys. Rev. D (to be published)].
[7] F. Herrmann, I. Hinder, D. M. Shoemaker, P. Laguna, and R. A. Matzner, Phys. Rev. D **76**, 084032 (2007).
[8] J. G. Baker, W. D. Boggs, J. Centrella, B. J. Kelly, S. T. McWilliams, M. C. Miller, and J. R. van Meter, Astrophys. J. **668**, 1140 (2007).
[9] M. Campanelli, C. O. Lousto, Y. Zlochower, and D. Merritt, Astrophys. J. **659**, L5 (2007).
[10] W. Tichy and P. Marronetti, Phys. Rev. D **76**, 061502(R) (2007).
[11] F. Herrmann, I. Hinder, D. Shoemaker, P. Laguna, and R. A. Matzner, arXiv:gr-qc/0701143.
[12] M. Koppitz, D. Pollney, C. Reisswig, L. Rezzolla, J. Thornburg, P. Diener, and E. Schnetter, Phys. Rev. Lett. **99**, 041102 (2007).
[13] D. Pollney *et al.*, Phys. Rev. D **76**, 124002 (2007).
[14] L. Rezzolla *et al.*, arXiv:0708.3999.
[15] M. Campanelli, C. O. Lousto, and Y. Zlochower, Phys. Rev. D **74**, 041501(R) (2006).
[16] P. Marronetti *et al.*, Phys. Rev. D **77**, 064010 (2008).
[17] M. Campanelli, C. O. Lousto, Y. Zlochower, B. Krishnan, and D. Merritt, Phys. Rev. D **75**, 064030 (2007).
[18] J. D. Schnittman and A. Buonanno, arXiv:astro-ph/0702641.
[19] T. Damour and A. Nagar, Phys. Rev. D **76**, 044003 (2007).
[20] J. D. Schnittman, Astrophys. J. **667**, L133 (2007).
[21] J. D. Schnittman *et al.*, Phys. Rev. D **77**, 044031 (2008).
[22] A. Buonanno, L. E. Kidder, and L. Lehner, Phys. Rev. D **77**, 026004 (2008).
[23] L. Rezzolla, P. Diener, E. N. Dorband, D. Pollney, C. Reisswig, E. Schnetter, and J. Seiler, Astrophys. J. **674**, L29 (2008).
[24] L. Boyle, M. Kesden, and S. Nissanke, Phys. Rev. Lett. **100**, 151101 (2008).
[25] LIGO, http://www.ligo.caltech.edu/.
[26] LISA, http://lisa.nasa.gov/.
[27] G. Kauffmann and M. Haehnelt, Mon. Not. R. Astron. Soc. **311**, 576 (2000).
[28] A. Cattaneo, Mon. Not. R. Astron. Soc. **324**, 128 (2001).
[29] A. Loeb, Phys. Rev. Lett. **99**, 041103 (2007).
[30] J. Dennett-Thorpe, P. A. G. Scheuer, R. A. Laing, A. H. Bridle, G. G. Pooley, and W. Reich, Mon. Not. R. Astron. Soc. **330**, 609 (2002).
[31] D. Merritt and R. D. Ekers, Science **297**, 1310 (2002).
[32] K. Gebhardt *et al.*, Astrophys. J. **539**, L13 (2000).
[33] S. Tremaine *et al.*, Astrophys. J. **574**, 740 (2002).
[34] M. Milosavljevic, D. Merritt, A. Rest, and F. C. van den Bosch, Mon. Not. R. Astron. Soc. **331**, L51 (2002).
[35] A. Gualandris and D. Merritt, arXiv:0708.0771.
[36] J. M. Bardeen, Nature (London) **226**, 64 (1970).
[37] K. S. Thorne, Astrophys. J. **191**, 507 (1974).
[38] L. Brenneman and C. Reynolds, Astrophys. J. **652**, 1028 (2006).
[39] J. M. Wang, Y. M. Chen, L. C. Ho, and R. J. McLure, Astrophys. J. **642**, L111 (2006).
[40] M. Elvis, G. Risaliti, and G. Zamorani, Astrophys. J. **565**, L75 (2002).
[41] T. Bogdanovic, C. Reynolds, and M. Miller, arXiv:astro-ph/0703054.
[42] J. D. Schnittman, Phys. Rev. D **70**, 124020 (2004).
[43] I. Hinder, B. Vaishnav, F. Herrmann, D. Shoemaker, and P. Laguna, Phys. Rev. D **77**, 081502 (2008).
[44] P. C. Peters and J. Mathews, Phys. Rev. **131**, 435 (1963).
[45] F. Pretorius and D. Khurana, Classical Quantum Gravity **24**, S83 (2007).
[46] J. D. Grigsby and G. B. Cook, Phys. Rev. D **77**, 044011 (2008).
[47] U. Sperhake, E. Berti, V. Cardoso, J. A. Gonzalez, B. Brugmann, and M. Ansorg, arXiv:0710.3823.
[48] M. C. Washik, J. Healy, F. Herrmann, I. Hinder, D. M. Shoemaker, P. Laguna, and R. A. Matzner, arXiv:0802.2520.
[49] L. E. Kidder, Phys. Rev. D **52**, 821 (1995).
[50] H. Tagoshi, A. Ohashi, and B. J. Owen, Phys. Rev. D **63**, 044006 (2001).
[51] G. Faye, L. Blanchet, and A. Buonanno, Phys. Rev. D **74**, 104033 (2006).

[52] L. Blanchet, A. Buonanno, and G. Faye, Phys. Rev. D **74**, 104034 (2006); **75**, 049903(E) (2007).
[53] M. J. Fitchett, Mon. Not. R. Astron. Soc. **203**, 1049 (1983).
[54] S. Dimopoulos and G. L. Landsberg, Phys. Rev. Lett. **87**, 161602 (2001).
[55] E. Berti, V. Cardoso, J. A. Gonzalez, U. Sperhake, and B. Brugmann, arXiv:0711.1097.
[56] A. Buonanno, G. B. Cook, and F. Pretorius, Phys. Rev. D **75**, 124018 (2007).
[57] A. Garat and R. H. Price, Phys. Rev. D **61**, 124011 (2000).
[58] J. D. Brown and J. W. York, Phys. Rev. D **47**, 1407 (1993).
[59] A. Ashtekar and B. Krishnan, Phys. Rev. D **68**, 104030 (2003).
[60] G. B. Cook and B. F. Whiting, Phys. Rev. D **76**, 041501 (2007).
[61] T. Chu, G. Lovelace, R. Owen, and H. Pfeiffer (unpublished).
[62] A. Lewis and S. Bridle, Phys. Rev. D **66**, 103511 (2002).